

Accepted Manuscript

Design, synthesis and biological evaluation of novel substituted purine isosters as EGFR kinase inhibitors, with promising pharmacokinetic profile and *in vivo* efficacy

Efthymios-Spyridon Gavriil, Aris Doukatas, Theodoros Karampelas, Vassilios Myriantopoulos, Spyridon Dimitrakis, Emmanuel Mikros, Panagiotis Marakos, Constantin Tamvakopoulos, Nicole Pouli

PII: S0223-5234(19)30439-8

DOI: <https://doi.org/10.1016/j.ejmech.2019.05.029>

Reference: EJMECH 11339

To appear in: *European Journal of Medicinal Chemistry*

Received Date: 29 March 2019

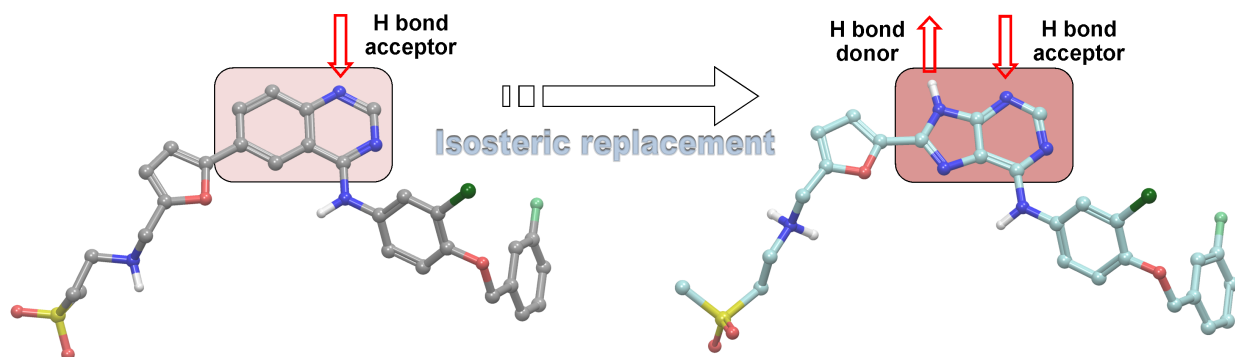
Revised Date: 7 May 2019

Accepted Date: 7 May 2019

Please cite this article as: E.-S. Gavriil, A. Doukatas, T. Karampelas, V. Myriantopoulos, S. Dimitrakis, E. Mikros, P. Marakos, C. Tamvakopoulos, N. Pouli, Design, synthesis and biological evaluation of novel substituted purine isosters as EGFR kinase inhibitors, with promising pharmacokinetic profile and *in vivo* efficacy, *European Journal of Medicinal Chemistry* (2019), doi: <https://doi.org/10.1016/j.ejmech.2019.05.029>.

This is a PDF file of an unedited manuscript that has been accepted for publication. As a service to our customers we are providing this early version of the manuscript. The manuscript will undergo copyediting, typesetting, and review of the resulting proof before it is published in its final form. Please note that during the production process errors may be discovered which could affect the content, and all legal disclaimers that apply to the journal pertain.





ACCEPTED MANUSCRIPT

Design, Synthesis and Biological Evaluation of Novel Substituted Purine Isosters as EGFR kinase inhibitors, with promising pharmacokinetic profile and in vivo efficacy.

Efthymios-Spyridon Gavriil,^{1§} Aris Doukatas,^{2§} Theodoros Karampelas,² Vassilios Myriantopoulos,¹ Spyridon Dimitrakis,¹ Emmanuel Mikros,¹ Panagiotis Marakos,¹ Constantin Tamvakopoulos,^{2*} Nicole Pouli^{1*}

¹ Division of Pharmaceutical Chemistry, Department of Pharmacy, School of Health Sciences, National and Kapodistrian University of Athens, Panepistimiopolis Zografou 15771, Athens, Greece

² Center of Clinical Research, Experimental Surgery and Translational Research, Biomedical Research Foundation Academy of Athens, Athens, Greece

Author Contributions

[§]The authors contributed equally.

*Correspondence to:

Nicole Pouli, e-mail: pouli@pharm.uoa.gr

Constantin Tamvakopoulos, e-mail: ctamvakop@bioacademy.gr

ABSTRACT

Novel substituted purine isosters, were designed and synthesized as potential inhibitors of the Epidermal Growth Factor Receptor (EGFR). The compounds were rationally designed through bioisosteric replacement of the central quinazoline core of lapatinib, an approved drug that inhibits both EGFR and HER2, another important member of this family of receptors. The new target molecules were evaluated as inhibitors of receptor phosphorylation at the cellular level, for their direct inhibitory action on the intracellular receptor kinase domain and for their cytotoxicity against the

non-small cell lung cancer cell line A549 and breast cancer HCC1954, cell lines which are associated with overexpression of EGFR and HER2, respectively. The most potent derivatives were further studied for their cellular uptake levels and *in vivo* pharmacokinetic properties. One compound (**23**) displayed a noteworthy pharmacokinetic profile, and higher intracellular accumulation in comparison to lapatinib in the A549 cells, possibly due to its higher lipophilicity. This lead compound (**23**) was assessed for its efficacy in an EGFR positive xenograft model, where it successfully inhibited tumor growth, with a similar efficacy with that of lapatinib and with minimal phenotypic toxicity.

Keywords: lapatinib, purine analogues, EGFR inhibitors, non-small cell lung cancer, breast cancer, pharmacokinetic studies

1. Introduction

The human epidermal growth factor family of cell surface receptors consists of four members (HER1-4, ErbB1-4), which serve as main mediators of cell signaling by extracellular growth factors and play key regulatory roles in essential cellular functions [1, 2]. They share the typical receptor tyrosine kinase architecture, with an extracellular ligand binding region, a single transmembrane segment and an intracellular tyrosine kinase domain [3]. Upon ligand binding, the receptors form homo and heterodimers and undergo a conformational change that activates the kinase domain, resulting in trans autophosphorylation and initiation of signal transduction cascades [4-7]. The abnormal overexpression or the presence of activating mutations of the HER family members cause malignant cell proliferation [8] and are implicated in a number of the most lethal solid tumors, such as non-small cell lung cancer (NSCLC), breast, ovarian, prostate, stomach, brain, colorectal cancer and melanoma [9-16]. Furthermore, increased levels of EGFR gene expression is particularly linked with higher cancer aggressiveness, tumor angiogenesis, postoperative adverse effects as well as with chemotherapy and radiotherapy resistance. Therefore, all existing data support the rationale for the development of antibody-based or small molecule inhibitors as EGFR-targeted therapeutics and presently, effective blockage of EGFR

and HER-2 has been clinically validated in cancer therapy. Monoclonal antibodies targeting the extracellular region of these receptors have been developed, with trastuzumab (Herceptin®) being the first one approved [17-21]. In parallel, several strategies involving small molecule tyrosine kinase inhibitors have been widely investigated in recent years resulting in six inhibitors approved so far, mainly targeting the EGFR (**Fig. 1**) [22-27]. All of the approved inhibitors act as ATP-competitive inhibitors and bind to the ATP binding site of EGFR, effectively preventing receptor phosphorylation and subsequent activation of downstream pathways. They share a central 4-anilinoquinazoline core, which serves as hinge adenine pocket binder, with the exception of osimertinib, which is structurally different, presenting instead, a core anilinoquinazoline scaffold. The first EGFR-targeted drugs are reversible inhibitors, offer great tolerability, and clinical outcome. However, the emergence of acquired resistance to treatment by the first generation inhibitors, prompted the discovery of next generation irreversible inhibitors such as afatinib (**Fig. 1**). Afatinib, bears an electrophilic functional group, capable of covalent Michael addition to a non- catalytic cysteine residue (Cys 797) of the enzyme [26]. Unfortunately, these drugs present a poor therapeutic window, as they are equally active against wild type and mutant EGFR [28].

On the other hand, recently approved third generation drugs exemplified by osimertinib (**Fig. 1**) are mutant selective irreversible inhibitors, capable of overcoming the previously observed toxicity limitations [27]. They bind covalently to Cys 797 and target different sensitizing EGFR mutant forms, including those harboring the gatekeeper T790M point mutation [29]. Despite initial encouraging results, additional resistance occurs rapidly, with one of the potential mechanisms being the appearance of additional EGFR mutations such as C797S [11, 30]. Consequently, continuous research efforts in this field are ongoing, aiming to discover new drug candidates in order to improve patient outcomes [31-34].

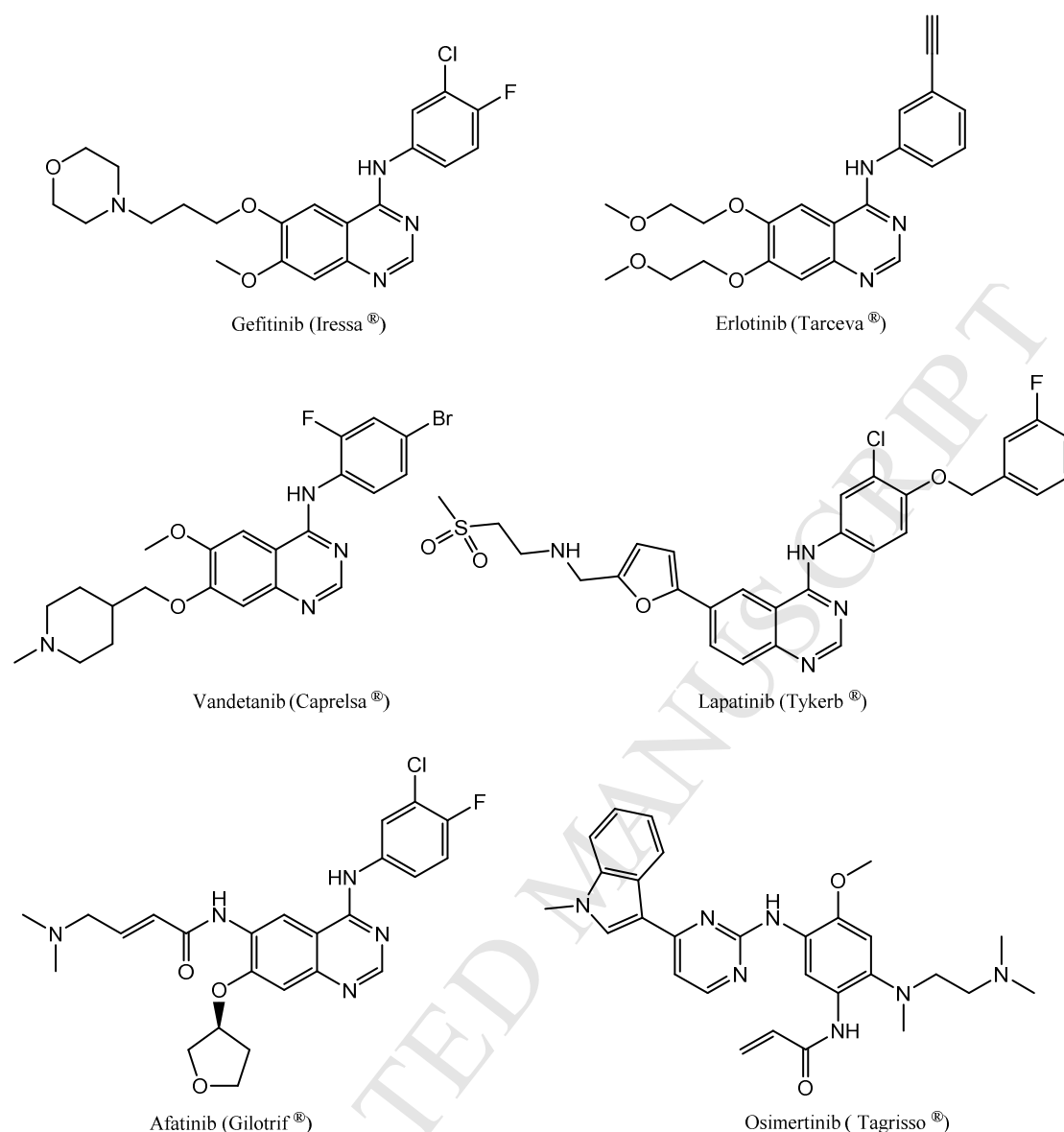


Fig. 1. Approved EGFR inhibitors.

Among the approved drugs, lapatinib (**Fig. 1**) bears a suitably selected 4-(3-fluorobenzoyloxy)-3-chloroanilino-substitution in order to act as dual EGFR/HER2 inhibitor [35-37]. It was developed based on the consideration that dual inhibition may lead to increased antitumor activity, since HER-2 overexpression potentiates EGFR signaling [38]. Indeed, lapatinib is indicated for HER2 overexpressing advanced or metastatic breast cancer [39, 40]. It is classified as I1/2 inhibitor, which binds reversibly to the inactive conformation of the EGFR kinase, displacing the characteristic α C-helix to the “out” conformation and giving the 3-fluorobenzoyloxy group access to the hydrophobic back pocket of the enzyme [41].

Taking into account the intriguing features of lapatinib and related inhibitors described in the literature [42-46], we have designed and synthesized a number of modified purines falling under the general formula presented in **Fig. 2**. All of them possess the hydrophobic 3-chloro-4-(3-fluorobenzoyloxy)anilino-group, which interacts with the selectivity pocket and extends into the back pocket of the enzyme, considered an essential feature for dual EGFR and HER2 inhibition. The central quinazoline core of lapatinib was replaced by purine isoster (**Fig. 2**, I-III) or purine (**Fig. 2**, IV) hinge binders. The hydrophilic and solvent exposed 5-substituted furan side chain of the drug was maintained, in order to optimize the drug-like properties of the molecules. In parallel, the corresponding 5-furyl-unsubstituted derivatives were synthesized, in order to evaluate the contribution of the furan side chain to the potency of the compounds.

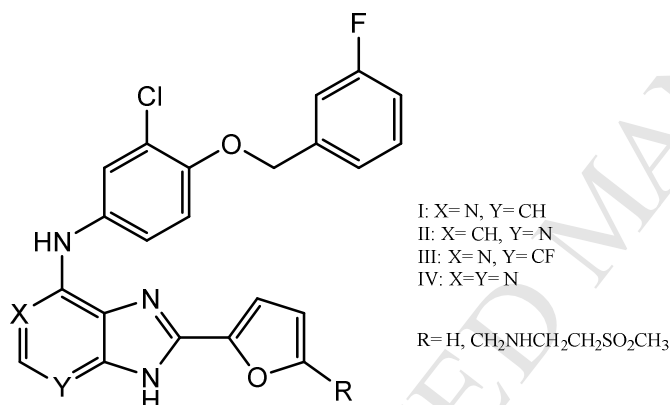


Fig. 2. General structure of the target compounds

2. Results and discussion

2.1. Theoretical studies

The design of the new analogues was based on the insight offered by the crystal structure of lapatinib in complex with EGFR (pdb id.: 1XKK). The inhibitor binds the inactive conformation of the kinase positioning the 3-fluorobenzoyloxy side-chain in a hydrophobic pocket formed next to the ATP binding pocket of the inactive-like kinase by rearrangement of α C helix (**Fig. 3A**). In this case, lapatinib is mainly stabilized in the kinase by a hydrogen bond formed at the enzyme hinge between the quinazoline nitrogen N1 and the backbone amide of M793, whereas most additional interactions

that contribute to the binding of the specific inhibitor are related to the substituents of the quinazoline scaffold. The crystallographic data show that the 3-fluorobenzyl group is critical for binding to the inactive kinase and hence for the inhibitor selectivity, as it facilitates cation- π and extensive stacking interactions accommodated within the additional pocket aside the binding site of the nucleotide. In a similar fashion, the methanesulfonyl group is exposed to a considerable extent to the solvent, further stabilizing the bound inhibitor by hydrogen bonds with polar sidechains of the protein surface, including D800, R803 and R841. The detailed inspection of the interaction mode between lapatinib and EGFR prompted the investigation of an isosteric replacement of the quinazoline core by a ring system with the capacity to accommodate additional hydrogen bonds with the kinase hinge. The imidazole-containing fused scaffolds I-IV (**Fig. 3B, 3C**) were considered based on the above strategy. Molecular simulations were performed and all four new scaffolds representing stepwise isosteric replacements were flexibly docked to the EGFR pocket and theoretically evaluated utilizing the Glide SP algorithm (Schrodinger Inc.) [47-49]. The purine scaffold IV was expected to provide a model for directly comparing the new isosteric heterocyclic system with lapatinib and assess whether an additional hydrogen bonding site could potentially interact with the backbone carbonyl of M793 in a bidentate fashion and further stabilize the inhibitor compared to the original active lead. Furthermore, the extent by which either of the two quinazoline nitrogens, N1 and N3, are critical for binding would be investigated from the permutation by an aromatic carbon in scaffolds I-II, whereas the addition of a fluorosubstituted carbon along the vector of the key hydrogen bonding interaction stabilizing lapatinib in EGFR would offer structural justification as to whether replacement of a hydrogen bond acceptor by a fluorine could have a favourable effect to binding. Likewise, to probe for the importance of the methanesulfonyl substituent to affinity, we prepared analogues that do not bear this group. Conversely, the anilino-substituent of the drug was maintained, as the molecular modelling results undoubtedly indicated its key importance for binding to the inactive state of EGFR, thus providing selectivity over similar kinase targets.

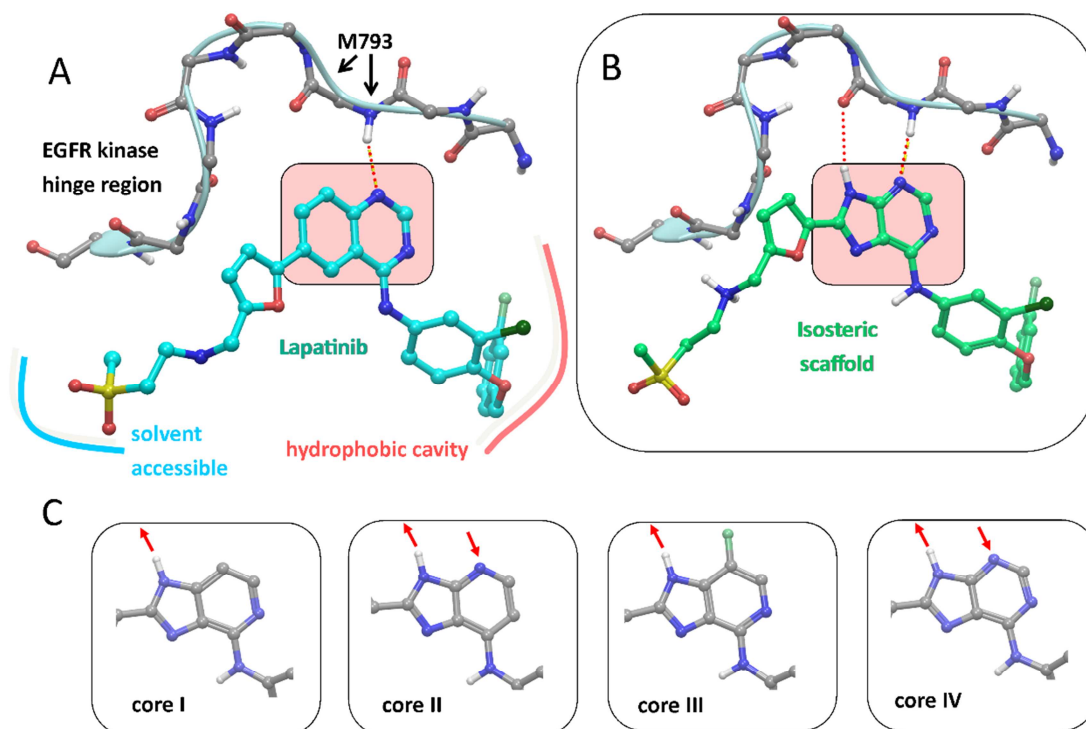
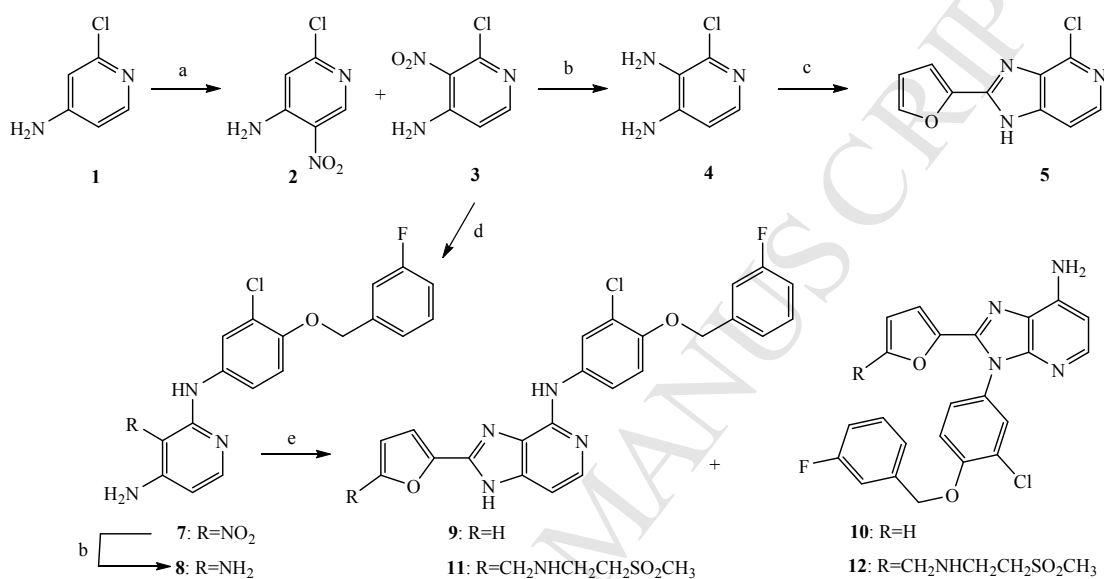


Fig. 3. **A)** A simplified depiction of the experimental binding mode of lapatinib in EGFR. The inhibitor anchors into the enzyme pocket through a hydrogen bond between the backbone of M793 and N1 of quinazoline whereas the 3-fluorobenzyloxy side-chain is oriented toward an adjacent to the active site hydrophobic cavity and the methanesulfonate group in the direction of bulk solvent. **B)** The designed isosteric modification of quinazoline into a purine-like system carried by the novel analogues aimed at achieving an additional hydrogen bond with respect to the original lead. **C)** The four distinct heterocyclic ring systems considered and evaluated in this study with the sites demonstrating hydrogen bond potential are depicted as red directed arrows.

2.2. Chemistry

In order to prepare compounds of the general structure I (**Fig. 2**), we used 4-amino-2-chloropyridine (**1**, **Scheme 1**) as starting material, which was nitrated and the resulting nitro-isomers **2** and **3** were chromatographically separated. Then, the 3-nitro derivative **3** was reduced to give the diamine **4**, which was ring-closed using 2-furancarbaldehyde, to provide the substituted imidazopyridine **5** [50, 51]. This compound was treated with 3-chloro-4-(3-fluorobenzyloxy)aniline (**6**), which was

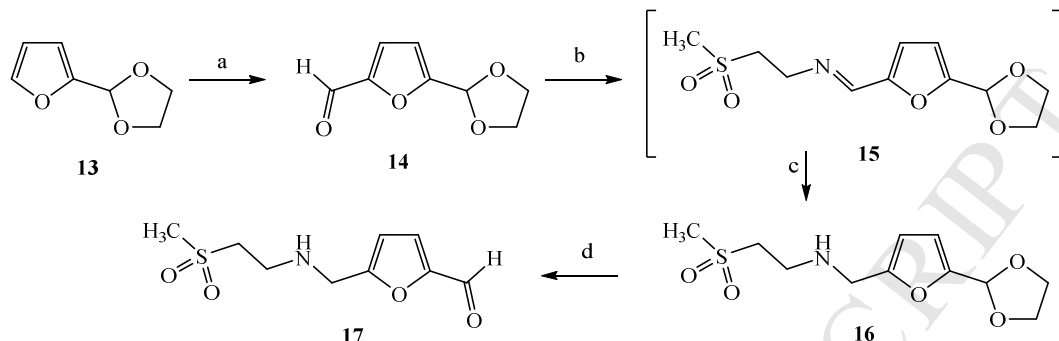
prepared according to a literature procedure, upon reaction of 2-chloro-4-nitrophenol with 3-fluorobenzylchloride and reduction of the resulting nitroderivative [45]. However, the attempted nucleophilic substitution was not successful, despite the variety of applied conditions (high temperature, microwave assistance, use of aniline anion).



Scheme 1. Reagents and conditions. a. HNO₃, H₂SO₄, 60°C, 4h; b. Zn, NH₄Cl, MeOH, 60°C, 2h; c. 2-furancarbaldehyde, DMSO, 100°C, 24h; d. 3-chloro-4-(3-fluorobenzoyloxy)aniline (**6**), Et₃N, EtOH, reflux, 8h; e. 2-furancarbaldehyde or **17**, DMSO, 100°C, 3h.

Consequently, the synthetic procedure was modified and the substituted aniline **6** was treated with the extremely reactive nitroderivative **3**, thus providing the substituted pyridine **7**. Compound **7** was then reduced and the resulting aminoderivative **8** was ring-closed using either 2-furancarbaldehyde, or freshly prepared suitably substituted carbaldehyde **17** (**Scheme 2**). The latter was prepared using the commercially available dioxolane **13**, which was converted to the carbaldehyde **14** following a literature procedure [52]. Compound **14** was then subjected to reductive amination using 2-(methylsulfonyl)ethylamine [45] followed by addition of sodiumborohydride

to give the furanacetal **16**. Acidic hydrolysis of the acetal resulted in the corresponding aldehyde **17**.



Scheme 2. Reagents and conditions. a. (i) LDA in THF/n-heptane/ethylbenzene 2.0M, DMF (dry), THF (dry), -78°C, 1h, (ii) rt, 24h; b. 2-(methylsulfonyl)ethylamine, Na₂SO₄, MeOH, reflux, 3h; c. NaBH₄, MeOH, rt, 2h; d. HCl 0.5N, CH₂Cl₂, rt, 1h.

The ring-closure of compound **8** (**Scheme 1**), provided the target imidazo[4,5-*c*]pyridines **9** and **11**, together with the isomeric 7-aminoimidazo[4,5-*b*]pyridines **10** and **12** respectively. Both isomers of each reaction were chromatographically separated and characterized.

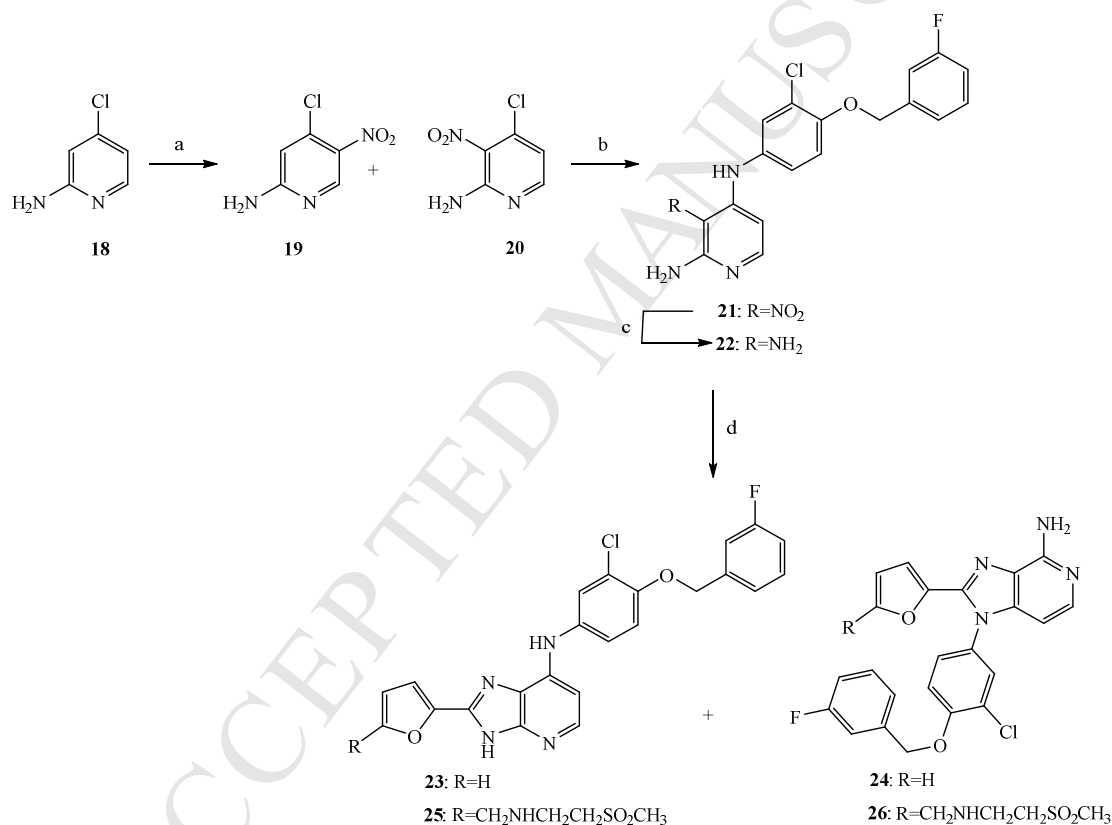
The conditions of the cyclization reaction were studied, concerning compounds **9** and **10**, applying a range of temperature values and reaction times (**Table 1**). It was assumed that the highest yield of the target product **9**, as well as the optimum ratio of **9** over **10** were achieved when the reaction was carried out at 100°C for 3h.

Table 1. Study of the cyclization reaction conditions.

Temperature	Yield of 9	Yield of 10	Ratio 9 / 10	Reaction time
Rt	10 %	62 %	1 / 6	24 h
70 °C	33 %	17 %	2 / 1	24 h

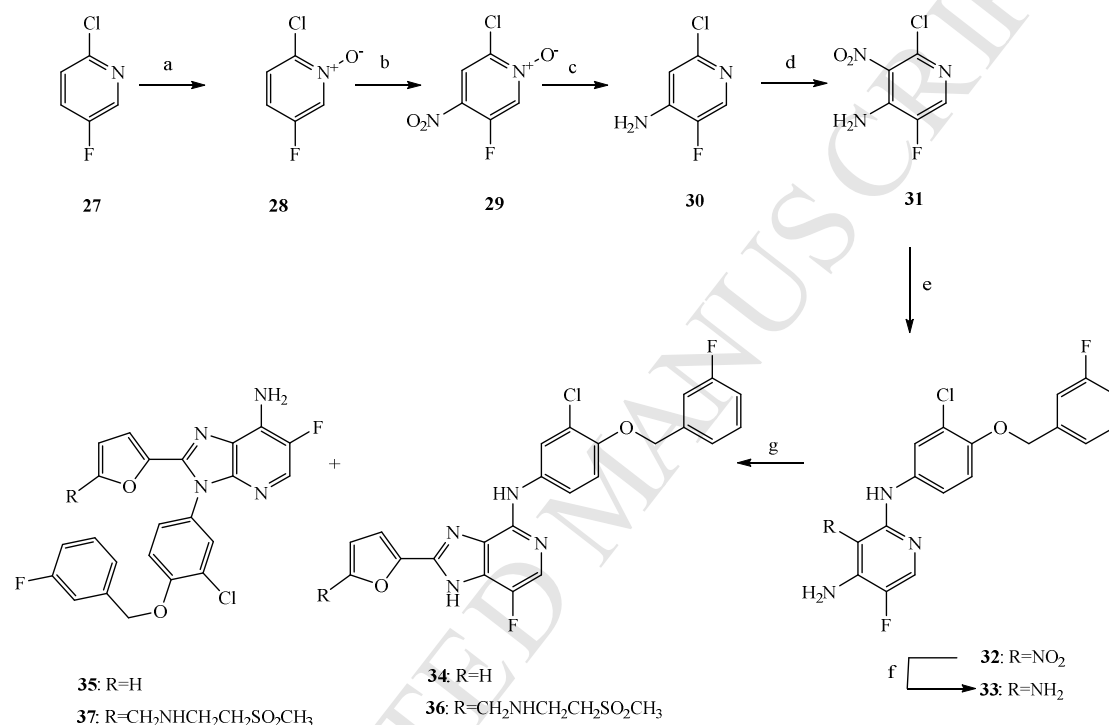
100 °C	34 %	10 %	3 / 1	3 h
130 °C	17 %	8 %	2 / 1	3 h

The second group of target compounds (compounds II, **Fig. 2**) was synthesized according to the above described procedure, using 2-amino-4-chloropyridine (**18**, **Scheme 3**) as starting material. This pyridine provided upon nitration both isomers **19** and **20** which were easily separated and identified [53]. Compounds **23** and **25**, together with the corresponding derivatives **24** and **26** were prepared accordingly from the nitroderivative **20**, and then separated and fully characterized.



Scheme 3. Reagents and conditions. a. HNO₃, H₂SO₄, 60°C, 4h; b. 3-chloro-4-(3-fluorobenzoyloxy)aniline (**6**), Et₃N, EtOH, reflux, 8h; c. Zn, NH₄Cl, MeOH, 60°C, 2h; d. 2-furancarbaldehyde or **17**, DMSO, 100°C, 3h.

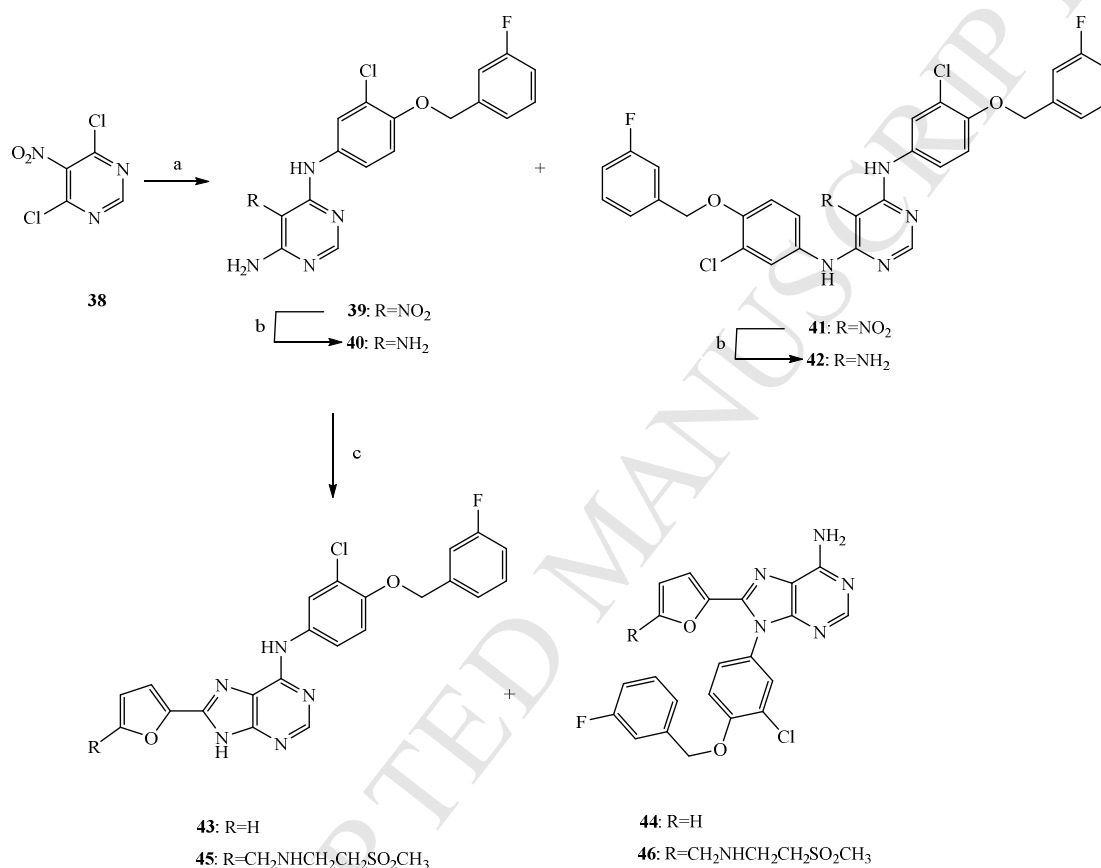
The synthesis of the fluorosubstituted analogues (compounds III, **Fig. 2**) was accomplished as depicted in **Scheme 4**, using 2-chloro-5-fluoropyridine (**27**). This compound was converted to the corresponding *N*-oxide **28**, which was successively nitrated and reduced to give the aminopyridine **30**. Following a second nitration step, this pyridine was converted to the nitro-compound **31** [54] that served as key intermediate for the preparation of the imidazopyridines **34** and **36**, which were obtained together with compounds **35** and **37** respectively.



Scheme 4. Reagents and conditions. a. H₂O₂ 30%, TFA, 70°C, 4h; b. KNO₃, H₂SO₄, 120°C, 2h; c. Fe, HCl, EtOH, reflux, 3h; d. KNO₃, H₂SO₄, rt, 24h; e. 3-chloro-4-(3-fluorobenzoyloxy)aniline (**6**), Et₃N, DMSO, 150°C, 24h; f. Zn, NH₄Cl, MeOH, 60°C, 2h; g. 2-furancarbaldehyde or **17**, DMSO, 100°C, 3h.

The synthesis of the purine analogues (compounds IV, **Fig. 2**) was performed according to the procedure illustrated in **Scheme 5**, starting from the nitropyrimidine **38**. This compound was treated in an one-pot reaction with the substituted aniline **6**, followed by the addition of ethanolic ammonia solution. This resulted in a mixture of compound **39**, together with an amount of the disubstituted derivative **41**. The chromatographic separation of these compounds proved to be very difficult, due to

their extremely low solubility, thus, only a small amount of each derivative was isolated in pure form using preparative thin layer chromatography, in order to elucidate their structure. The mixture was introduced to the next, reduction step and the aminoderivatives, **40** and **42**, were isolated in pure form. Compound **40** was then used for the preparation of the target derivatives **43** and **45**, which resulted together with **44** and **46**, following the previously described methodology.



Scheme 5. Reagents and conditions. a. (i) 3-chloro-4-(3-fluorobenzoyloxy)aniline (**6**), NaHCO₃, EtOH, 70°C, 1h (ii) NH₃ in EtOH 4M, 70°C, 2h; b. Zn, NH₄Cl, MeOH, 60°C, 2h; c. 2-furancarbaldehyde or **17**, DMSO, 100°C, 3h.

2.3. Inhibition of Isolated Kinase and cell-based Phosphorylation Inhibition

The *in vitro* kinase inhibitory activity of the eight new compounds against EGFR was evaluated using a biochemical assay measuring their ability to inhibit EGFR autophosphorylation. The autophosphorylation inhibition potential of the derivatives in comparison with lapatinib was investigated at two representative concentrations of

10 μM and 1 μM (**Fig. 4**). Three compounds showed potent inhibitory activity against EGFR (**11**, **23** and **45**), with the effect being in direct comparison to corresponding inhibition levels obtained by lapatinib.

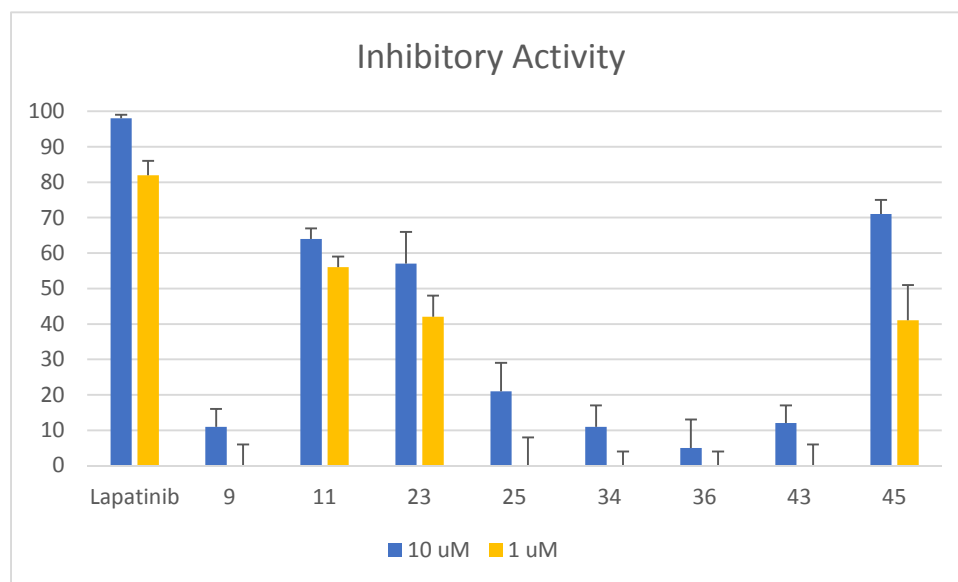


Fig. 4. EGFR-TK inhibitory activity of lapatinib and tested compounds derived by the *in vitro* evaluation of the EGFR inhibitory activity in isolated enzyme. Compounds were tested in duplicate and the reported % EGFR-TK inhibition represents the average of three independent experiments (\pm SD).

Inhibition of phosphorylation of EGFR by the new compounds was further assessed in the NSCLC cell line A549 and in the BrCa cell line HCC-1954, using a Western Blot based assay (**Fig. 5**). Four derivatives (**45**, **25**, **23** and **11**) were found to possess interesting inhibitory potencies, both in cell-free and cell-based experiments. The compounds were also evaluated against the closely related HER2 kinase and **9** demonstrated the highest potency compared to lapatinib, followed by **43** (**Table S1**). The ability of the compounds to inhibit HER2 phosphorylation in cells was also investigated at two representative concentrations of 2 μM and 0.02 μM . Four compounds (**11**, **25**, **36** and **43**) displayed the highest potencies compared to lapatinib (**Fig. S1**).

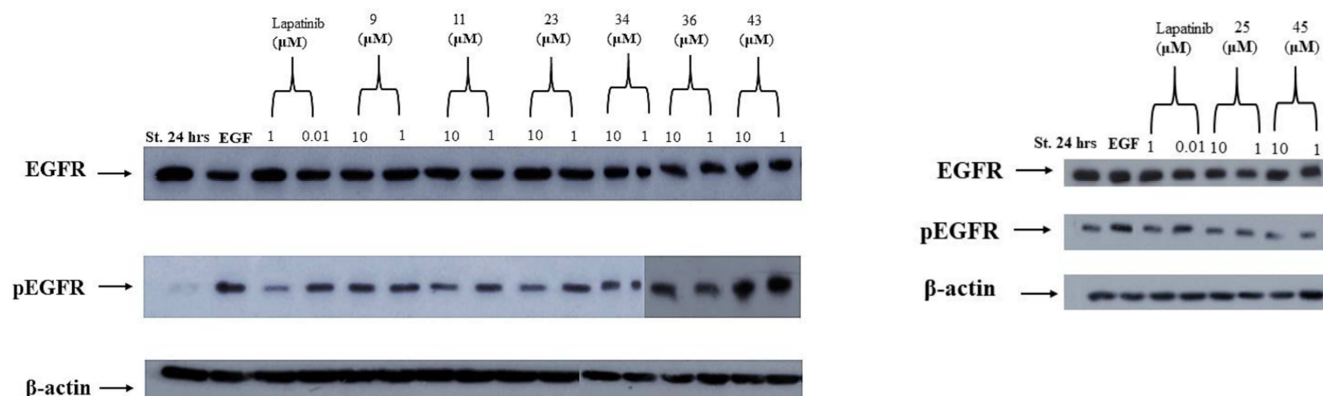


Fig. 5. In vitro inhibition of the phosphorylation of EGFR in A549 cells by Lapatinib (1 μ M & 0.01 μ M) and the new analogues (10 μ M & 1 μ M).

2.4. Docking simulations

Flexible docking calculations using the Embrace module of Maestro were performed to provide a possible explanation for the observed activity of the new derivatives [55]. With respect to the most active compounds **45** and **23**, docking suggested that indeed the N9 of novel cores II and IV demonstrates high predicted capacity to form an additional hydrogen bond inside the kinase, in agreement with the rational design discussed previously. This particular hydrogen bond is anticipated to further stabilize the purine analogues in the enzyme pocket (**Fig. 6**) and possibly counterbalance unfavorable entropic contributions originating from the restructuring of the water network that might result by the isosteric replacement, thus preserving the original kinase inhibitory potency of the quinazoline lead. Moreover, simulations provided a clear explanation for the diminished inhibition of core III and the fluorosubstituted derivatives **34** and **36**, as this limited structural modification resulted in the disruption of one out of the two hydrogen bonds stabilizing the ligand into the protein cavity. Nevertheless, docking failed to fully explain the effect of the methanesulfonate substituent of cores I and II to EGFR kinase binding affinity, with the results indicating the chain bearing derivatives **11** and **25** as more active than their counterparts **9** and **23**, in contrast to the *in vitro* results suggesting that more than one

binding geometries may be involved. Of note, the derived binding modes of the new derivatives were regarded of high confidence, as their predicted binding geometries demonstrated excellent agreement with the original lapatinib mode (**Fig. 6**).

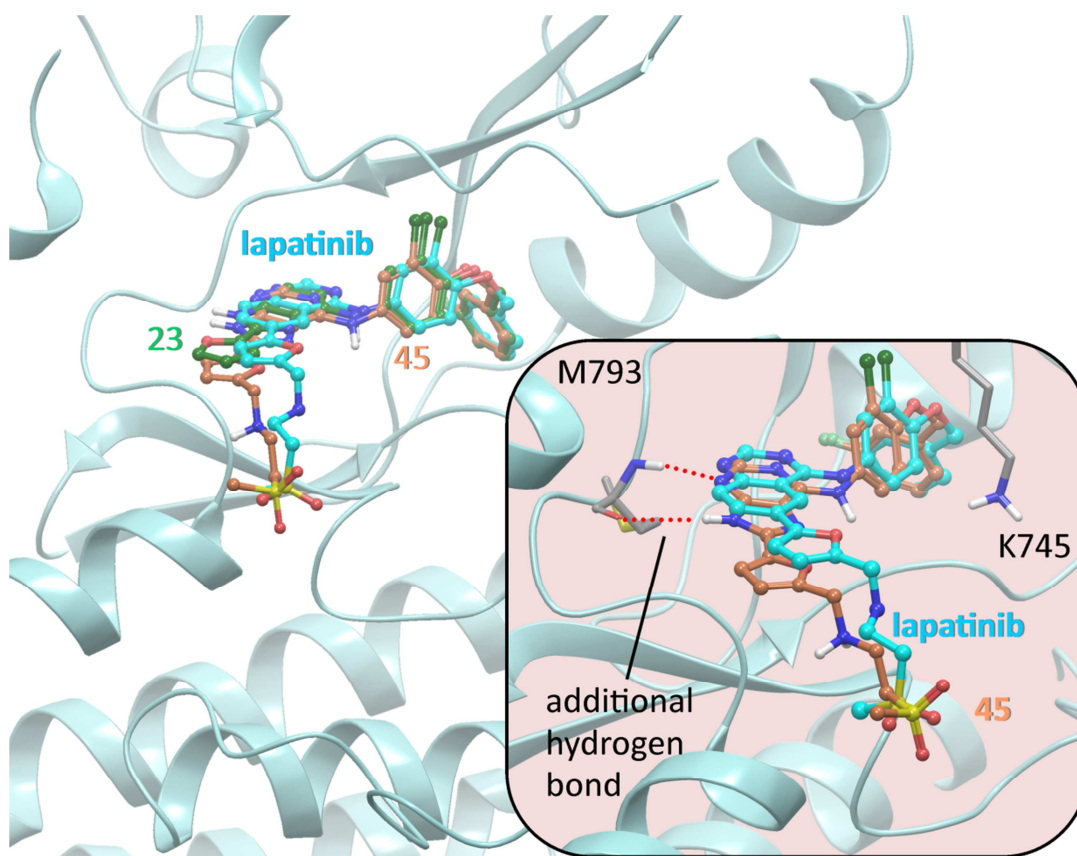


Fig. 6. A superposition of the crystallographic binding mode of lapatinib (cyan carbons, pbd id: 1XKK) and the predicted modes of active analogues **23** (green carbons) and **45** (orange carbons) as derived by docking calculations inside the EGFR kinase domain in a ribbon representation of the protein. In the inset, a detailed representation of the additional hydrogen bond hypothesized to further stabilize the newly synthesized derivatives bearing an imidazopyridine (**23**) or purine scaffold (**45**) at the kinase hinge, in comparison to the isosteric quinazoline core accommodating only one favorable interaction inside the cavity of EGFR.

2.5. *In vitro* cytotoxic effect

The antiproliferative activity of the new compounds was investigated in the NSCLC cell line A549 and in the BrCa cell line HCC-1954 using lapatinib as the reference

compound (**Fig. 7 a,b** and **Fig. S2**). Four representative concentrations (60 μ M, 40 μ M, 10 μ M and 1 μ M) were used in order to identify the most potent compounds, based on their overall cytotoxicity. Three compounds (**43**, **23** and **45**) were found to possess high cytotoxicities against both A549 and HCC-1954 cell lines (**Fig. 7 a,b**). Overall, based on the *in vitro* evaluation results, derivatives **23** and **45** were selected for further *in vitro* and pharmacokinetic evaluation in mice. These compounds were potent inhibitors of EGFR phosphorylation (ELISA and Western blot assays) and at the same time cytotoxic against both cell lines (A549 and HCC-1954). On the other hand, compound **9** was found to display inhibitory effect in the biochemical tyrosine kinase pHER2 assay, whereas **25** was found potent inhibitor in the Western Blot Assay. However, neither of the two compounds showed strong antiproliferative activity against the two cell lines (A549 and HCC-1954).

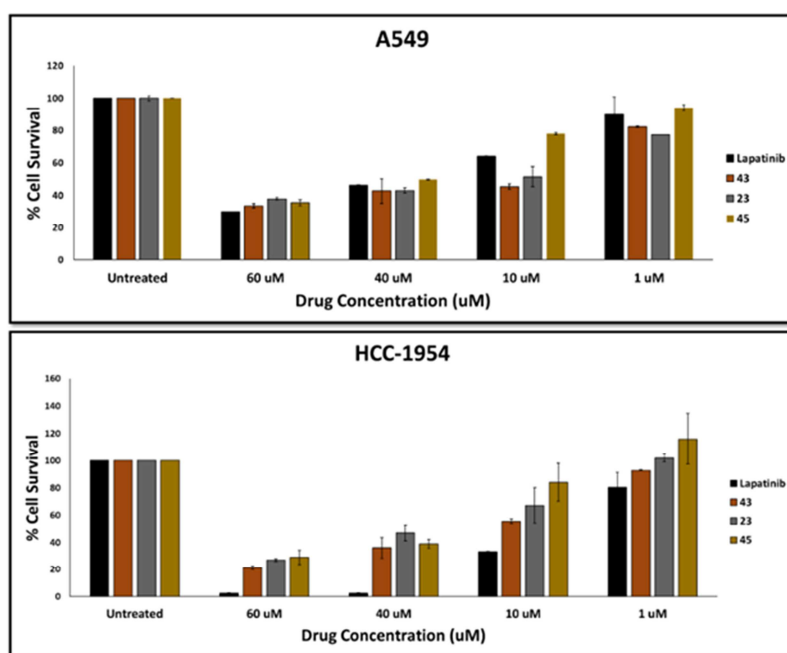


Fig. 7. Antiproliferative activity of lapatinib and selected potent new derivatives was evaluated in (a) A549 and (b) HCC-1954 cells (60 μ M, 40 μ M, 10 μ M & 1 μ M) by MTT cytotoxicity assay.

The full antiproliferative activity profile of the two selected compounds (**23** and **45**) was further evaluated in comparison to lapatinib in the two NSCLC cell lines A549

and NCI-H1975 and the two BrCa cell lines HCC-1954 and MCF-7. Comparative IC₅₀ values are presented in **Table 2**.

Table 2. Antiproliferative effect of lapatinib, **23** and **45** against NSCLC cell lines A549 and NCI-H1975 and BrCa cell lines HCC-1954 and MCF-7.

Cell lines	IC ₅₀ values (μM)*		
	Lapatinib	23	45
A549	11 (±2)	3 (±1)	33 (±10)
NCI-H1975	9 (±1)	10 (±3)	30 (±6)
HCC-1954	5 (±1)	9 (±3)	14 (±6)
MCF-7	95 (±9)	126 (±13)	105 (±10)

*Each IC₅₀ value is the average of three independent experiments performed in triplicate (±SD).

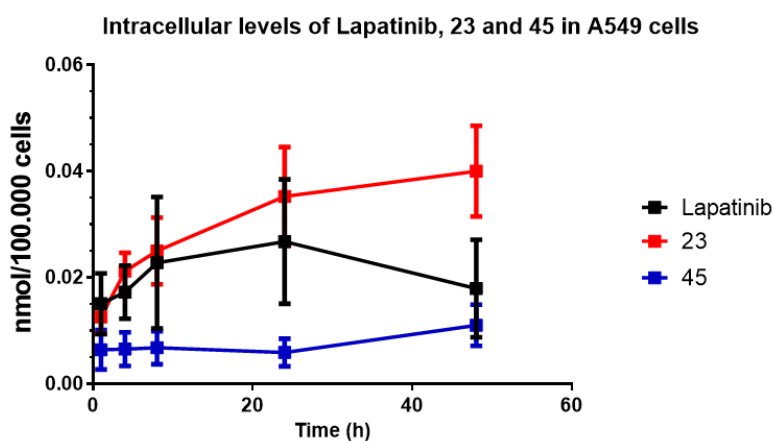
2.6. Characterization of selected compounds using Liquid Chromatography-Mass Spectrometry (LC-MS/MS) and Prediction of Key Efficacy Related Properties

LC-MS/MS characterization and method development-optimization was used for the detection and quantification of lapatinib and the two selected compounds (**23** and **45**). The identification of the characteristics of mass spec (MS) features (precursor and product ions, table S2) helped us to proceed with the *in vitro* and *in vivo* studies that were performed in order to assess the biological features of the molecules under investigation (i.e. cellular uptake, *in vivo* biodistribution). Selective LC-MRM (multiple reaction monitoring) methods were developed for the three compounds (lapatinib, **23**, **45**) based on their characteristic MS features and the methodologies were validated in the matrix of interest (i.e. cells collected from cell culture or mouse blood) with respect to limit of quantification, linearity, and reproducibility. The developed methodologies were utilized in cell uptake studies and pharmacokinetic

evaluation of lapatinib and the two compounds. In addition, *in silico* predictions were made for some key molecular properties concerning the efficacy of these compounds (Table S2). Among them, **23** displayed higher cLogP (4.7) than lapatinib and **45** (3.7 and 2.9 respectively) therefore being the most lipophilic, while its polar surface area was 67.2 \AA^2 ($<100 \text{ \AA}^2$), a desired feature for drug candidates, known to influence cell membrane permeability [56].

2.7. Cell uptake of **23** and **45** in A549 cells

The cell uptake of **23** and **45** in A549 cells was evaluated in comparison to lapatinib (Fig. 8). Compound **23** exhibited higher cellular uptake in A549 cells than lapatinib, especially with respect to the late time points of 24h and 48h of incubation time ($AUC_{(1-48h)}$: 1.5 nmol/100.000 cells x h versus $AUC_{(1-48h)}$: 1.06 nmol/100.000 cells x h for lapatinib). It could be suggested that the physicochemical properties of this compound (higher lipophilicity, lower total polar surface area) are responsible for its higher accumulation [57].



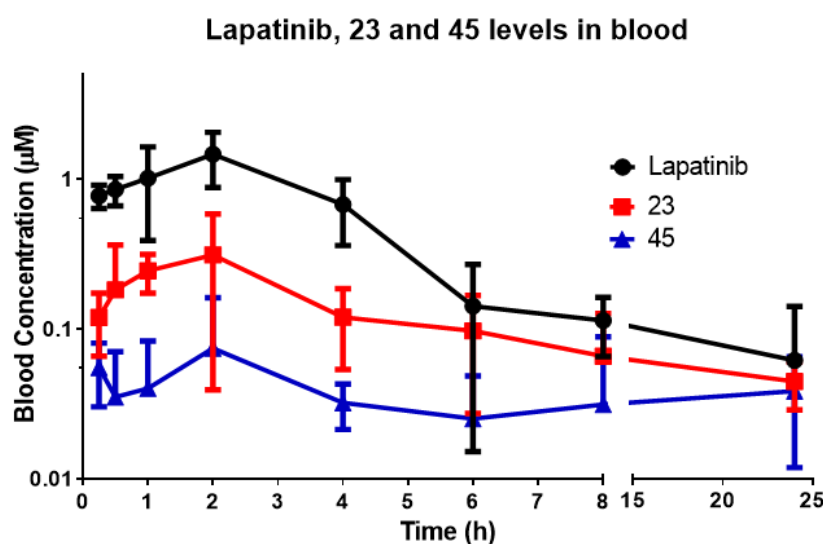
Compounds	Levels at 48h (nmol/100.000 cells)	$AUC_{(1-48h)}$ (nmol/100.000 cells x h)
Lapatinib	0.02 (± 0.01)	1.06 (± 0.30)
23	0.04 (± 0.01)	1.50 (± 0.20)
45	0.01	0.35 (± 0.10)

Fig. 8. Cellular uptake of **23** and **45** in the NSCLC cell line A549, in comparison to Lapatinib. Cells were incubated with 1 μ M Lapatinib, **23** and **45** for selected time points (1h, 4h, 8h, 24h and 48h) and were then lysed in order to determine

intracellular levels of the three compounds by LC-MS/MS. Experiments were performed in triplicate (\pm SD)

2.8. Pharmacokinetic evaluation of **23** and **45**

Assessment of the *in vivo* pharmacokinetics (PK) of the two selected compounds (**23** and **45**) was performed in mice. The PK parameters of both molecules were compared to lapatinib after oral administration, using an identical solubilizing vehicle and an equimolar dose of 34 μ mol/kg (**Fig. 9**). Lapatinib maximum concentration in blood was achieved at 2h post administration (1.47 μ M) with an $AUC_{(0-24h)}$ of 6.7 \times h \times μ M. Similarly, **23** and **45** reached highest blood concentrations at 2h post administration (0.30 μ M and 0.07 μ M for **45**). Overall, both compounds had no advantages over lapatinib in oral dosing. However, the pharmacokinetic experiment was used as a guide for subsequent studies for compound **23**. From the two compounds, **23** had only marginally improved bioavailability compared to **45** ($AUC_{(0-24h)}$ of 2.1 h \times μ M for **23** compared to 0.87 \times h \times μ M for **45**). Based on the above mentioned data, **23** was selected as lead candidate for subsequent efficacy studies in mice.



Compounds	Oral Dose (mg/kg)	Equimolar Oral Dose (μ mol/kg)	Cmax (μ M)	tmax (h)	$AUC_{(0h-24h)}$ (h \times μ M)
Lapatinib	20	34	1.47 (\pm 0.30)	2	6.70 (\pm 2.50)
23	14.8	34	0.30 (\pm 0.10)	2	2.10 (\pm 1.40)
45	19.4	34	0.07 (\pm 0.04)	2	0.87 (\pm 0.60)

Fig. 9. Pharmacokinetic evaluation of **23** and **45** versus Lapatinib. Male C57BL/6N mice ($n = 5$) were dosed orally with either Lapatinib, **23** or **45** at a dose of $34 \mu\text{mol/kg}$ and blood samples were collected at selected time points. Lapatinib, **23** and **45** levels were monitored by LC-MS/MS. The areas under the curve (AUCs) for each treatment were calculated as a measure of drug exposure over time (\pm SD).

2.9. *In vivo* antitumor efficacy of **23** and Lapatinib

The efficacy of **23** was evaluated on a EGFR positive xenograft lung cancer model using the NSCLC A549 cell line. Efficacy was compared to equimolar dose of lapatinib under a selected dosing scheme ($86 \mu\text{mol/kg}$, once daily oral administration). Pharmacological treatment with either lapatinib or **23** was initiated when tumors reached approximately 150 mm^3 and was continued for a total period of 27 days. At the end of the treatment period (day 27), the average tumor volume in mice treated with **23** ($1311 \pm 458 \text{ mm}^3$, $P = 0.01$) or with lapatinib ($1338 \pm 358 \text{ mm}^3$, $P = 0.001$) was significantly lower compared to the size of tumors for vehicle ($1869 \pm 134 \text{ mm}^3$) mice (**Fig. 10a**) suggesting that the two compounds (lapatinib and **23**) have similar efficacy profiles in the specific animal model. No signs of discomfort or evidence of drug-induced toxicity was observed as measured by changes in animal total body weight (**Fig. 10b**). Concentrations of lapatinib and **23** in blood and tumor tissue were measured at 2 h after the final dose. Lapatinib's blood concentrations were $2.81 \mu\text{M}$, whereas the blood levels of **23** were $0.64 \mu\text{M}$ (**Fig. 10c**). These results are consistent with the pharmacokinetic evaluation of the two compounds, where an equimolar dose of $34 \mu\text{mol/kg}$ was used. Although, we were able to measure lapatinib levels in tumor tissue, levels of compound **23** had great variation, possibly due to a different tumor uptake profile due to its different physiochemical properties that could lead to differences in the tumor uptake mechanisms (e.g. P-gp efflux, passive diffusion) or the formation of metabolites that couldn't be identified.

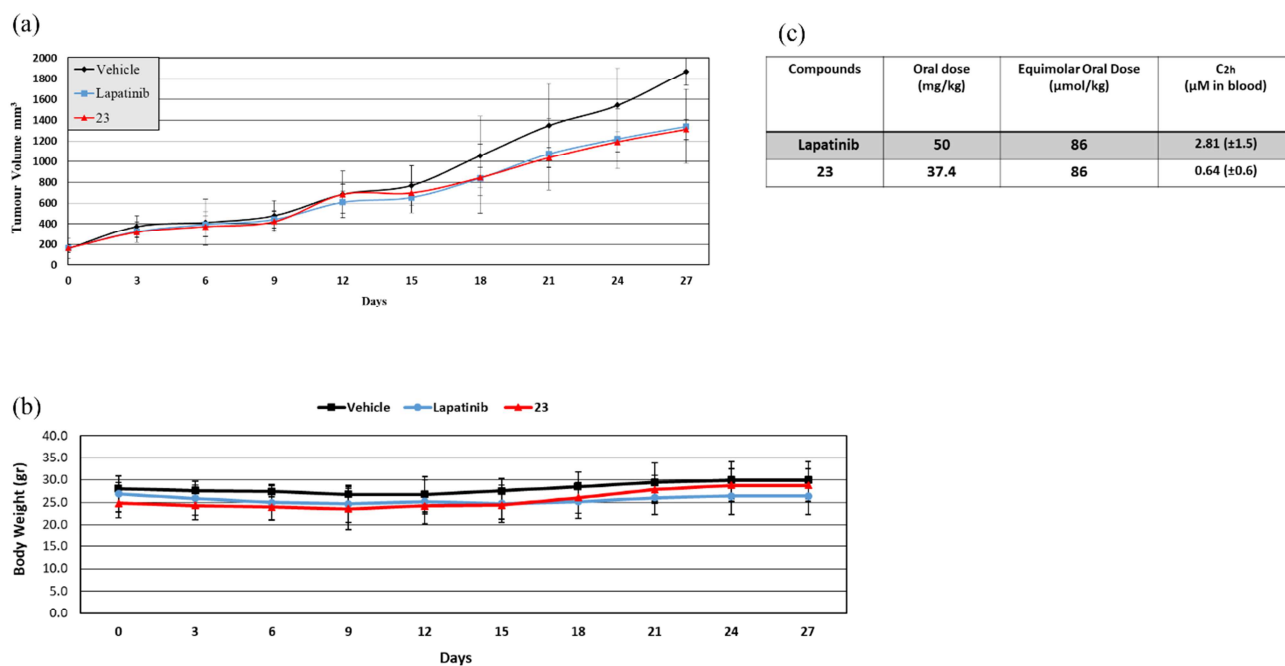


Figure 10. Therapeutic efficacy of **23**. (a) Tumor growth inhibition in NOD/SCID mice xenografted with A549 cells and treated with daily gavage administration of **23**, lapatinib and vehicle. Each point represents the mean of at least 8 tumor volumes resulting from at least 4 mice \pm SD ***, $P < 0.001$ vs controls and \pm SD **, $P < 0.01$ vs controls. (b) Absence of toxicity was assessed by total body weight measurements of all treated mice. (c) Average blood drug concentrations were measured by LC-MS/MS at 2h post a final dose on d27, (\pm SD).

Overall, this study deals with the synthesis, biological and pharmacokinetic evaluation of a number of new lapatinib analogues, designed to assess the potential of applying rationally selected isosteric replacements on the lead quinazoline core of the drug. The results could assist in expanding the SAR landscape of EGFR inhibition and, moreover probe for the importance of specific structural features on the activity against the target kinase. The *in vitro* evaluation of the synthesized compounds in a cell free assay showed that derivative **45**, possessing a purine central core instead of the quinazoline ring of lapatinib, showed a highly promising efficacy, which was perfectly anticipated by docking simulations. Replacement of the quinazoline N1 by a fluorosubstituted carbon perturbed the pharmacophoric hydrogen bond acceptor and thus resulted in inactive analogues (**34**, **36**). However, a consistent trend with respect to the presence of the furan side chain on inhibition potency could not be established, as **23** and **11** were determined to be equally active against EGFR kinase, regardless of their difference with respect to the aforementioned substitution. In addition, the corresponding derivatives **25** (carrying substitution on the furan ring) and **9** (without substitution) both showed diminished potency.

To further confirm the biological activities obtained in the isolated enzyme, the inhibitory activity of the novel derivatives against EGFR was carried out in a cell-based assay. The observed inhibitory effect of the new analogues on EGFR autophosphorylation was in good agreement with the results obtained at the cell free assay as **11**, **23** and **45** were the most effective in inhibiting phospho-EGFR formation, with the exception of derivative **25**. In order to study the effect that the new analogues could exert on cell proliferation, the same cells were treated with the synthesized compounds and their cytotoxic effect was measured, showing that **23**, **43** and **45** were the most potent in this respect. Whereas two of the compounds, **23** and **45**, were well expected to exert potent cytotoxic results based on their already confirmed EGFR inhibition potency, the discrepancy between the EGFR inhibitory potential and cytotoxic potency of **43** was an indication of considerable off-target activities, possibly leading to the observed cytotoxicity. In light of those observed biological responses and aiming to assist the evaluation, the antiproliferative effect of the most promising derivatives **23** and **45** was studied in a more extensive protocol using relevant cell lines, in order to obtain a more detailed description of the *in vitro* cytotoxic landscape of the studied molecules. Compound **23** exhibited higher potency than **45** in both NSCLC cell lines, as well as against BrCa cell line HCC-1954, and most importantly it displayed greater potency ($IC_{50} = 3 \mu M$) compared to lapatinib ($IC_{50} = 11 \mu M$) in the A549 cell line. In line with lapatinib, those two compounds could not inhibit strongly MCF-7 cell proliferation, presenting comparable IC_{50} values, approximately equal to $100 \mu M$. As this breast cancer cell line does not express EGFR, the finding suggests that both compounds could be regarded as considerably selective for EGFR. **24** and **45** were then subsequently assessed for their bioavailability and cellular uptake and **23** resulted in high measured levels, both in cells and blood, suggesting that **23** could lead to more sustainable intracellular levels, compared to lapatinib. Importantly, the improved pharmacokinetic profile of **23** was in line with the more relevant drug-like physicochemical properties such as cLogP of the specific substance. Thus, **23** could be perceived as a valuable drug candidate, with enhanced tumor bioavailability, more importantly considering the comparable *in vivo* efficacy to lapatinib.

3. Conclusion

In conclusion, we have designed and synthesized a new series of lapatinib analogues, inducing modifications in the central quinazoline core and taking care to preserve, or not extensively modify, the original substituents of the drug. The chemical procedure for the preparation of the compounds involved the use of a suitable aminonitrochloropyridine (or pyrimidine), which was first substituted with a preformed aniline and then reduced and ring-closed upon reaction with selected furancarbaldehydes. This procedure resulted in the preparation of a series of corresponding isomeric side-products as well, bearing a primary amino-group, thus considered as adenine isosters. These compounds were also introduced in the primary screening tests, albeit they did not possess interesting inhibitory activity against EGFR in the biochemical assays and thus, were not further investigated. Following the evaluation of the biochemical and cellular activity of the target compounds against EGFR and HER2, two derivatives, **23** and **45** were selected for further *in vitro* and *in vivo* evaluation. We have shown that **23** had greater potency than lapatinib against the A549 cells based on the cell toxicity studies. Importantly, **23** presented satisfactory pharmacokinetic properties and higher intracellular levels than lapatinib in the A549 cells, possibly due to its higher lipophilicity and enhanced tumor penetration. The *in vivo* efficacy study of **23** in an EGFR xenograft animal model showed that it can successfully inhibit tumor growth, with a similar efficacy profile with that of lapatinib and with minimal phenotypic toxicity.

In conclusion, compound **23** possessing an altered, nitrogen rich central scaffold compared to lapatinib, is a potent and promising novel anticancer compound with adequate physiochemical properties and interesting biological activity in EGFR inhibition.

4. Experimental Section

4.1. Chemistry

Melting points were determined on a Büchi apparatus and are uncorrected. ^1H NMR spectra and 2D spectra were recorded on a Bruker Avance III 600 or a Bruker Avance DRX 400 instrument, whereas ^{13}C NMR spectra were recorded on a Bruker Avance III 600 or a Bruker AC 200 spectrometer in deuterated solvents and were referenced

to TMS (δ scale). The signals of ^1H and ^{13}C spectra were unambiguously assigned by using 2D NMR techniques: $^1\text{H}^1\text{H}$ COSY, NOESY, HMQC, and HMBC. Mass spectra were recorded with a LTQ Orbitrap Discovery instrument, possessing an Ionmax ionization source. Flash chromatography was performed on Merck silica gel 60 (0.040 - 0.063 mm). Analytical thin layer chromatography (TLC) was carried out on precoated (0.25 mm) Merck silica gel F-254 plates.

4.1.1. 4-Chloro-2-(furan-2-yl)-1H-imidazo[4,5-c]pyridine (5). To a solution of compound **4** (300 mg, 2.09 mmol)[51] in dimethylsulfoxide (1.0 mL) was added under Ar a solution of 2-furaldehyde in dimethylsulfoxide (0.5 mL, 2.09 mmol) and the mixture was heated at 100 °C for 24 h. The solvent was then vacuum-evaporated and the residue was purified using silica gel column chromatography (cyclohexane/ethyl acetate: 1/2), in order to provide **5** as a light brown solid (240 mg, 52%). M.p. > 215 °C dec. (Et_2O). ^1H NMR (600 MHz, $\text{DMSO}-d_6$) δ 13.95-13.35 (brs, 1H, NH), 8.11 (d, $J = 5.5$ Hz, 1H, H-6), 8.03 (dd, $J = 1.8, 0.6$ Hz, 1H, H-5'), 7.55 (d, $J = 5.5$ Hz, 1H, H-7), 7.39 (d, $J = 3.4$ Hz, 1H, H-3'), 6.78 (dd, $J = 3.4, 1.8$ Hz, 1H, H-4'). ^{13}C NMR (151 MHz, $\text{DMSO}-d_6$) δ 145.90 (C-5'), 144.27 (C-2'), 141.99 (C-2), 141.60 (C-4), 141.01 (C-6), 139.44 (C-7a), 136.98 (C-3a), 112.92 (C-3'), 112.70 (C-4'), 107.95 (C-7).

4.1.2. 2-N-[3-Chloro-4-(3-fluorobenzoyloxy)phenyl]-3-nitropyridine-2,4-diamine (7). To a solution of the pyridine **3** (300 mg, 1.73 mmol)[51] in absolute ethanol (10 mL) were added triethylamine (0.5 mL, 3.58 mmol) and the aniline **6** (500 mg, 1.99 mmol)[45] and the mixture was heated at reflux for 8 h. The solvent was vacuum-evaporated, water was added to the residue and the precipitate was filtered, washed with water, dried and purified using silica gel column chromatography (dichloromethane) to give pure **7** (440 mg, 65%). M.p. = 159-160 °C (EtOAc/n -hexane). ^1H NMR (400 MHz, $\text{DMSO}-d_6$) δ 10.39 (s, 1H, NH), 8.20 (s, 2H, NH_2), 7.91 (d, $J = 2.4$ Hz, 1H, H-2'), 7.69 (d, $J = 5.9$ Hz, 1H, H-6), 7.46 (m, 2H, H-6', H-5''), 7.30 (m, 2H, H-2'', H-6''), 7.17 (m, 2H, H-5', H-4''), 6.30 (d, $J = 5.9$ Hz, 1H, H-5), 5.22 (s, 2H, CH_2). ^{13}C NMR (151 MHz, $\text{DMSO}-d_6$) δ 162.99, 161.37 (C-3''), 153.04 (C-2), 151.53 (C-4), 149.88 (C-6), 149.58 (C-4'), 139.71, 139.66 (C-1''), 133.10 (C-

1'), 130.55, 130.49 (C-5''), 124.30 (C-2'), 123.26 (C-6''), 122.50 (C-6'), 121.05 (C-3'), 116.50 (C-3), 114.71, 114.57 (C-4''), 114.27 (C-5'), 114.03, 113.89 (C-2''), 103.77 (C-5), 69.35 (CH₂).

4.1.3. *2-N-[3-Chloro-4-(3-fluorobenzyloxy)phenyl]pyridine-2,3,4-triamine (8)*. To a solution of the nitroderivative **7** (900 mg, 2.32 mmol) in methanol (10 mL) were added zinc dust (2.60 g, 39.8 mmol) and ammonium chloride (2.90 g, 54.2 mmol) and the mixture was heated at 60 °C for 2 h. It was then filtered through a celite pad and the filtrate was concentrated under vacuum. The residue was purified by silica gel column chromatography (CH₂Cl₂/MeOH: 85/15) to give **8** as an oil (600 mg, Yield: 72%). ¹H NMR (600 MHz, DMSO-*d*₆) δ 7.76 (d, *J* = 2.6 Hz, 1H, H-2'), 7.59 (s, 1H, NH), 7.44 (m, 1H, H-5''), 7.33 (dd, *J* = 9.0, 2.6 Hz, 1H, H-6'), 7.31-7.26 (m, 3H, H-6, H-2'', H-6''), 7.15 (m, 1H, H-4''), 7.07 (d, *J* = 9.0 Hz, 1H, H-5'), 6.20 (d, *J* = 5.4 Hz, 1H, H-5), 5.36 (s, 2H, 4-NH₂), 5.14 (s, 2H, CH₂), 4.13 (s, 2H, 3-NH₂). ¹³C NMR (151 MHz, DMSO-*d*₆) δ 162.99, 161.38 (C-3''), 146.47 (C-4'), 143.87 (C-2), 142.39 (C-4), 140.09, 140.04 (C-1''), 137.83 (C-1'), 136.22 (C-6), 130.47, 130.42 (C-5''), 123.28 (C-6''), 121.44 (C-3'), 119.01 (C-2'), 117.34 (C-6'), 115.24 (C-5'), 115.17 (C-3), 114.60, 114.47 (C-4''), 114.04, 113.89 (C-2''), 104.58 (C-5), 69.74 (CH₂).

4.1.4. *N-[3-Chloro-4-(3-fluorobenzyloxy)phenyl]-2-(furan-2-yl)-1H-imidazo[4,5-*c*]pyridin-4-amine (9) and 3-[3-chloro-4-(3-fluorobenzyloxy)phenyl]-2-(furan-2-yl)-3H-imidazo[4,5-*b*]pyridin-7-amine (10)*. To a solution of **8** (120 mg, 0.33 mmol) in dimethylsulfoxide (1.0 mL) was added under Ar a solution of 2-furaldehyde (28 μL, 0.34 mmol) in dimethylsulfoxide (0.1 mL) and the resulting solution was heated at 100 °C in a preheated oilbath for 3 h. The solvent was vacuum-evaporated and the residue was purified using silica gel column chromatography (cyclohexane/EtOAc: 1/2), to provide both isomers, which were separated using preparative thin layer chromatography (cyclohexane/EtOAc: 2/3).

Data for **9**: 50 mg, 34%, M.p. = 110-111 °C (MeOH). ¹H NMR (400 MHz, DMSO-*d*₆) δ 13.21 (s, 1H, imidazole NH), 9.13 (s, 1H, aniline NH), 8.33 (d, *J* = 2.5 Hz, 1H, H-2'), 7.96 (d, *J* = 1.3 Hz, 1H, H-5''), 7.87 (m, 2H, H-6, H-6'), 7.45 (m, 1H, H-5''),

7.31 (m, 2H, H-2'', H-6''), 7.20 (d, $J = 3.4$ Hz, 1H, H-3'''), 7.15 (m, 2H, H-5', H-4''), 6.96 (d, $J = 5.7$ Hz, 1H, H-7), 6.75 (dd, $J = 3.4, 1.3$ Hz, 1H, H-4'''), 5.19 (s, 2H, CH₂). ¹³C NMR (50 MHz, DMSO-*d*₆) δ 164.62, 159.78 (C-3''), 147.58 (C-4), 147.39 (C-4'), 145.08 (C-2'''), 144.72 (C-5'''), 142.11 (C-2), 140.08, 139.93 (C-1''), 139.75 (C-6), 138.65 (C-7a), 136.06 (C-1'), 130.58, 130.41 (C-5''), 128.14 (C-3a), 123.28 (C-6''), 121.14 (C-3'), 120.34 (C-2'), 118.71 (C-6'), 114.79 (C-5'), 114.79, 114.37 (C-4''), 114.20, 113.77 (C-2''), 112.36 (C-4'''), 110.62 (C-3'''), 99.77 (C-7), 69.56 (CH₂). HR-MS (ESI) m/z : calcd for C₂₃H₁₇ClFN₄O₂, [M+H]⁺ = 435.1019, found 435.1010.

Data for **10**: 15 mg, 10%, M.p. = 200-201 °C (EtOAc/*n*-hexane). ¹H NMR (400 MHz, DMSO-*d*₆) δ 7.80 (s, 1H, H-5'''), 7.74 (d, $J = 5.4$ Hz, 1H, H-5), 7.67 (s, 1H, H-2'), 7.50 (m, 1H, H-5''), 7.41 (m, 2H, H-5', H-6'), 7.36 (m, 2H, H-2'', H-6''), 7.21 (m, 1H, H-4''), 6.58 (brs, 2H, NH₂), 6.55 (s, 1H, H-4'''), 6.42 (d, $J = 5.4$ Hz, 1H, H-6), 6.20 (d, $J = 3.1$ Hz, 1H, H-3'''), 5.36 (s, 2H, CH₂). ¹³C NMR (151 MHz, DMSO-*d*₆) δ 163.03, 161.42 (C-3''), 153.79 (C-4'), 149.46 (C-3a), 146.90 (C-7), 145.16 (C-5), 144.55 (C-5'''), 144.26 (C-2'''), 140.20 (C-2), 139.26, 139.21 (C-1''), 130.67, 130.62 (C-5''), 129.90 (C-2'), 128.82 (C-1'), 128.47 (C-6'), 123.42 (C-6''), 122.33 (C-7a), 121.79 (C-3'), 114.92, 114.78 (C-4''), 114.46 (C-5'), 114.21, 114.07 (C-2''), 111.78 (C-4'''), 111.64 (C-3'''), 103.09 (C-6), 69.52 (CH₂). HR-MS (ESI) m/z : calcd for C₂₃H₁₅ClFN₄O₂, [M-H]⁻ = 433.0862, found 433.0876.

4.1.5. 2-{5-[2-(Methylsulfonyl)ethylamino]methyl}furan-2-yl}-1,3-dioxolane (**16**). To a solution of carbaldehyde **14** (310 mg, 1.85 mmol)[52] in dry methanol (7.0 mL) were added under Ar sodium sulfate (1.20 g, 8.45 mmol) followed by 2-(methylsulfonyl)ethylamine (310 mg, 2.52 mmol) and the mixture was heated at reflux for 3 h. Then, the reaction was allowed to return at rt, sodium borohydride (370 mg, 9.78 mmol) was added under cooling and stirring continued at rt for 2 h. The solvent was vacuum-evaporated, water was added to the residue and it was extracted with dichloromethane. The organic layers were dried (sodium sulfate) and evaporated to dryness to give pure **16** as a yellow oil (500 mg, 98%). ¹H NMR (600 MHz, DMSO-*d*₆) δ 6.44 (d, $J = 3.1$ Hz, 1H, H-4), 6.24 (d, $J = 3.1$ Hz, 1H, H-3), 5.81 (s, 1H, H-2'), 4.03 – 3.88 (m, 4H, H-4', H-5'), 3.68 (s, 2H, CH₂(a)), 3.21 (t, $J = 6.6$ Hz, 2H,

CH₂(c)), 3.00 (s, 3H, CH₃), 2.91 (t, *J* = 6.6 Hz, 2H, CH₂(b)), 2.40 – 2.30 (brs, 1H, NH). ¹³C NMR (151 MHz, DMSO-*d*₆) δ 154.66 (C-2), 149.87 (C-5), 109.58 (C-4), 107.28 (C-3), 96.80 (C-2'), 64.46 (C-4', C-5'), 53.60 (CH₂(c)), 44.95 (CH₂(a)), 42.05 (CH₂(b)), 41.45 (CH₃).

4.1.6. 5-{{2-(Methylsulfonyl)ethylamino}methyl}furan-2-carboxaldehyde (**17**). A 0.5N HCl solution (5.0 mL, 2.5 mmol) was added dropwise under cooling to a solution of the acetal **16** (220 mg, 0.80 mmol) in dichloromethane (10 mL) and the mixture was stirred vigorously at rt for 1 h. Then, a 25% ammonium hydroxide solution was added until pH 11-12. Upon extraction with dichloromethane, the organic layer was dried (sodium sulfate) and evaporated to dryness to provide pure **17** as a yellow oil (170 mg, 93%). ¹H NMR (600 MHz, DMSO-*d*₆) δ 9.52 (s, 1H, CHO), 7.49 (d, *J* = 3.5 Hz, 1H, H-3), 6.60 (d, *J* = 3.5 Hz, 1H, H-4), 3.82 (s, 2H, CH₂(a)), 3.24 (t, *J* = 6.7 Hz, 2H, CH₂(c)), 3.00 (s, 3H, CH₃), 2.93 (t, *J* = 6.7 Hz, 2H, CH₂(b)). ¹³C NMR (151 MHz, DMSO-*d*₆) δ 177.72 (CHO), 161.34 (C-5), 151.75 (C-2), 124.61 (C-3), 110.05 (C-4), 53.59 (CH₂(c)), 45.02 (CH₂(a)), 42.12 (CH₂(b)), 41.51 (CH₃).

4.1.7. *N*-[3-Chloro-4-(3-fluorobenzyloxy)phenyl]-2-{5-[2-(methylsulfonyl)ethylaminomethyl]furan-2-yl}-1*H*-imidazo[4,5-*c*]pyridin-4-amine (**11**) and 3-[3-chloro-4-(3-fluorobenzyloxy)phenyl]-2-{5-[2-(methylsulfonyl)ethylaminomethyl]furan-2-yl}-3*H*-imidazo[4,5-*b*]pyridin-7-amine (**12**). These compounds were prepared using a methodology analogous to that of **9** and **10** respectively and purified first by silica gel column chromatography (EtOAc/MeOH: 8/2) resulting to a mixture of both products, which were then isolated pure using semi-preparative reverse phase high performance liquid chromatography (H₂O/MeOH: 2/8 to 1/9).

Data for **11**: 30 mg, Yield: 20%, M.p. = 101-102 °C (MeOH). ¹H NMR (600 MHz, DMSO-*d*₆) δ 13.56 – 12.56 (brs, 1H, imidazole NH), 8.97 (s, 1H, aniline NH), 8.33 (d, *J* = 2.5 Hz, 1H, H-2'), 7.82 (m, 2H, H-6, H-6'), 7.46 (m, 1H, H-5''), 7.31 (m, 2H, H-2'', H-6''), 7.19 – 7.06 (m, 3H, H-5', H-4'', H-3'''), 6.94 (d, *J* = 5.6 Hz, 1H, H-7), 6.51 (d, *J* = 3.1 Hz, 1H, H-4'''), 5.19 (s, 2H, OCH₂), 3.83 (s, 2H, CH₂(a)), 3.27 (t, *J* =

6.8 Hz, 2H, CH₂(c)), 3.02 (s, 3H, CH₃), 2.98 (t, $J = 6.8$ Hz, 2H, CH₂(b)), 2.48 – 2.40 (brs, 1H, ethylamine NH). ¹³C NMR (151 MHz, DMSO-*d*₆) δ 163.04, 161.43 (C-3''), 156.14 (C-5'''), 147.51 (C-4), 147.41 (C-4'), 144.10 (C-2'''), 142.25 (C-2), 140.05, 140.01 (C-1''), 139.72 (C-6), 138.70 (C-7a), 136.11 (C-1'), 130.57, 130.52 (C-5''), 128.22 (C-3a), 123.35 (C-6''), 121.21 (C-3'), 120.33 (C-2'), 118.70 (C-6'), 114.88 (C-5'), 114.70, 114.56 (C-4''), 114.09, 113.95 (C-2''), 111.49 (C-3'''), 109.56 (C-4'''), 99.83 (C-7), 69.60 (OCH₂), 53.67 (CH₂(c)), 45.14 (CH₂(a)), 42.12 (CH₂(b)), 41.49 (CH₃). HR-MS (ESI) m/z : calcd for C₂₇H₂₄ClFN₅O₄S, [M-H]⁻ = 568.1216, found 568.1193.

Data for **12**: 10 mg. Oil. Yield: 7%. ¹H NMR (600 MHz, DMSO-*d*₆) δ 7.73 (d, $J = 5.5$ Hz, 1H, H-5), 7.66 (m, 1H, H-2'), 7.50 (m, 1H, H-5''), 7.40 (m, 2H, H-5', H-6'), 7.35 (m, 2H, H-2'', H-6''), 7.21 (m, 1H, H-4''), 6.53 (brs, 2H, NH₂), 6.41 (d, $J = 5.5$ Hz, 1H, H-6), 6.33 (d, $J = 3.4$ Hz, 1H, H-4'''), 6.00 (d, $J = 3.4$ Hz, 1H, H-3'''), 5.37 (s, 2H, OCH₂), 3.69 (s, 2H, CH₂(a)), 3.21 (t, $J = 6.6$ Hz, 2H, CH₂(c)), 3.00 (s, 3H, CH₃), 2.90 (t, $J = 6.6$ Hz, 2H, CH₂(b)), 2.35 – 2.29 (brs, 1H, NH). ¹³C NMR (151 MHz, DMSO-*d*₆) δ 163.07, 161.46 (C-3''), 155.92 (C-5'''), 153.85 (C-4'), 149.73 (C-7), 146.74 (C-3a), 145.27 (C-5), 143.21 (C-2'''), 140.29 (C-2), 139.29, 139.24 (C-1''), 130.73, 130.67 (C-5''), 130.05 (C-2'), 128.91 (C-1'), 128.63 (C-6'), 123.47 (C-6''), 122.34 (C-7a), 121.87 (C-3'), 114.97, 114.83 (C-4'), 114.57 (C-5'), 114.25, 114.10 (C-2''), 112.35 (C-3'''), 108.92 (C-4'''), 103.14 (C-6), 69.56 (OCH₂), 53.65 (CH₂(c)), 44.93 (CH₂(a)), 42.08 (CH₂(b)), 41.55 (CH₃). HR-MS (ESI) m/z : calcd for C₂₇H₂₆ClFN₅O₄S, [M+H]⁺ = 570.1373, found 570.1346.

4.1.8. 4-*N*-[3-Chloro-4-(3-fluorobenzyloxy)phenyl]-3-nitropyridine-2,4-diamine (**21**).

This compound was prepared using a methodology analogous to that of **7**, starting from the aminopyridine **20** [53]. The compound was purified by silica gel column chromatography (CH₂Cl₂/MeOH: 95/5). Yield: 89%. M.p. > 210 °C dec. (EtOAc/*n*-hexane). ¹H NMR (600 MHz, DMSO-*d*₆) δ 10.06 (s, 1H, NH), 7.86 (s, 2H, NH₂), 7.69 (d, $J = 5.9$ Hz, 1H, H-6), 7.50 – 7.45 (m, 2H, H-2', H-5''), 7.34 – 7.25 (m, 4H, H-5', H-6', H-2'', H-6''), 7.18 (m, 1H, H-4''), 5.91 (d, $J = 5.9$ Hz, 1H, H-5), 5.27 (s, 2H, CH₂). ¹³C NMR (151 MHz, DMSO-*d*₆) δ 163.02, 161.40 (C-3''), 156.16 (C-2), 153.00 (C-6), 151.89 (C-4'), 150.51 (C-4), 139.44, 139.39 (C-1''), 131.78 (C-1'),

130.65, 130.59 (C-5''), 128.01 (C-2'), 126.33 (C-6'), 123.36 (C-6''), 121.88 (C-3'), 116.46 (C-3), 114.85, 114.73 (C-4''), 114.73 (C-5'), 114.13, 113.98 (C-2''), 98.05 (C-5), 69.40 (CH₂).

4.1.9. *4-N-[3-Chloro-4-(3-fluorobenzyloxy)phenyl]pyridine-2,3,4-triamine (22)*. This compound was prepared using a methodology analogous to that of **8**. The compound was purified using silica gel column chromatography (CH₂Cl₂/MeOH: 85/15) and obtained as an oil. Yield: 72%. ¹H NMR (600 MHz, DMSO-*d*₆) δ 8.45 (s, 1H, NH), 7.46 (m, 1H, H-5''), 7.33 – 7.27 (m, 4H, H-6, H-2', H-2'', H-6''), 7.25 (d, *J* = 8.9 Hz, 1H, H-5'), 7.17 (m, 1H, H-4''), 7.14 (dd, *J* = 8.9, 2.6 Hz, 1H, H-6'), 6.93 (s, 2H, 2-NH₂), 6.39 (d, *J* = 7.0 Hz, 1H, H-5), 5.23 (s, 2H, CH₂), 4.94 (s, 2H, 3-NH₂). ¹³C NMR (151 MHz, DMSO-*d*₆) δ 163.07, 161.45 (C-3''), 150.43 (C-4'), 143.33 (C-2), 140.51 (C-4), 139.61, 139.56 (C-1''), 133.46 (C-1'), 130.69, 130.63 (C-5''), 126.23 (C-6), 124.79 (C-2'), 123.40 (C-6''), 123.04 (C-6'), 122.14 (C-3'), 115.22 (C-5'), 114.93 (C-3), 114.87, 114.74 (C-4''), 114.15, 114.00 (C-2''), 100.79 (C-5), 69.57 (CH₂).

4.1.10. *N-[3-Chloro-4-(3-fluorobenzyloxy)phenyl]-2-(furan-2-yl)-3H-imidazo[4,5-*b*]pyridin-7-amine (23) and 1-[3-chloro-4-(3-fluorobenzyloxy)phenyl]-2-(furan-2-yl)-1H-imidazo[4,5-*c*]pyridin-4-amine (24)*. These compounds were prepared using a methodology analogous to that of **9** and **10** respectively and purified first by silica gel column chromatography (CH₂Cl₂/MeOH: 95/5 to 8/2) resulting to a mixture of both products, which were then isolated pure using preparative thin layer chromatography (CH₂Cl₂/MeOH: 93/7).

Data for **23**: Yield: 26%, M.p. = 190-191 °C (Et₂O). ¹H NMR (600 MHz, DMSO-*d*₆) δ 13.23 (s, 1H, imidazole NH), 8.99 (s, 1H, aniline NH), 7.94 (d, *J* = 4.5 Hz, 1H, H-5), 7.91 (s, 1H, H-5'''), 7.47 (m, 2H, H-6', H-5''), 7.32 (m, 3H, H-2', H-2'', H-6''), 7.23 (d, *J* = 8.8 Hz, 1H, H-5'), 7.19 (m, 2H, H-4'', H-3'''), 6.71 (m, 2H, H-6, H-4'''), 5.23 (s, 2H, CH₂). ¹³C NMR (151 MHz, DMSO-*d*₆) δ 163.01, 161.40 (C-3''), 149.32 (C-4'), 145.73 (C-2'''), 145.11 (C-5), 144.59 (C-5'''), 142.21 (C-3a), 142.16 (C-7), 139.76, 139.71 (C-1''), 134.69 (C-1'), 130.59, 130.53 (C-5''), 124.60 (C-7a), 123.42 (C-6'), 123.31 (C-6''), 121.83 (C-3'), 121.41 (C-2'), 115.01 (C-5'), 114.75, 114.61

(C-4''), 114.08, 113.93 (C-2''), 112.20 (C-4'''), 110.45 (C-3'''), 99.95 (C-6), 69.52 (CH₂). HR-MS (ESI) *m/z*: calcd for C₂₃H₁₅ClFN₄O₂, [M-H]⁻ = 433.0862, found 433.0878.

Data for **24**: Yield: 13%. M.p. = 195-196 °C (Et₂O). ¹H NMR (600 MHz, DMSO-*d*₆) δ 7.80 (d, *J* = 1.4 Hz, 1H, H-5'''), 7.77 (d, *J* = 2.5 Hz, 1H, H-2'), 7.68 (d, *J* = 5.8 Hz, 1H, H-6), 7.53 – 7.48 (m, 2H, H-6', H-5''), 7.46 (d, *J* = 8.8 Hz, 1H, H-5'), 7.37 (m, 2H, H-2'', H-6''), 7.22 (m, 1H, H-4''), 6.58 (brs, 2H, NH₂), 6.56 (dd, *J* = 3.5, 1.4 Hz, 1H, H-4'''), 6.34 (d, *J* = 5.8 Hz, 1H, H-7), 6.22 (d, *J* = 3.5 Hz, 1H, H-3'''), 5.36 (s, 2H, CH₂). ¹³C NMR (151 MHz, DMSO-*d*₆) δ 163.04, 161.42 (C-3''), 154.27 (C-4'), 152.00 (C-4), 144.78 (C-5'''), 143.82 (C-2'''), 141.80 (C-6), 141.45 (C-7a), 140.85 (C-2), 139.12, 139.07 (C-1''), 130.70, 130.65 (C-5''), 129.30 (C-2'), 128.83 (C-1'), 127.91 (C-6'), 125.60 (C-3a), 123.58 (C-6''), 122.26 (C-3'), 115.00, 114.85 (C-4''), 114.85 (C-5'), 114.34, 114.20 (C-2''), 111.98 (C-3'''), 111.87 (C-4'''), 96.12 (C-7), 69.65 (CH₂). HR-MS (ESI) *m/z*: calcd for C₂₃H₁₅ClFN₄O₂, [M-H]⁻ = 433.0862, found 433.0878.

4.1.11. *N*-[3-Chloro-4-(3-fluorobenzyloxy)phenyl]-2-{5-[2-(methylsulfonyl)ethylaminomethyl]furan-2-yl}-3*H*-imidazo[4,5-*b*]pyridin-7-amine (25) and *1*-[3-chloro-4-(3-fluorobenzyloxy)phenyl]-2-{5-[2-(methylsulfonyl)ethylaminomethyl]furan-2-yl}-1*H*-imidazo[4,5-*c*]pyridin-4-amine (26). These compounds were prepared using a methodology analogous to that of **9** and **10** respectively and purified first by silica gel column chromatography (CH₂Cl₂/MeOH: 95/5 to 8/2) resulting to a mixture of both products, which were then isolated pure using preparative thin layer chromatography (CH₂Cl₂/MeOH: 9/1).

Data for **25**: Yield: 10%. M.p. = 124-125 °C (Et₂O). ¹H NMR (600 MHz, DMSO-*d*₆) δ 13.38 – 13.00 (brs, 1H, imidazole NH), 9.00 (s, 1H, aniline NH), 7.93 (d, *J* = 5.6 Hz, 1H, H-5), 7.47 (m, 2H, H-2', H-5''), 7.32 (m, 3H, H-6', H-2'', H-6''), 7.23 (d, *J* = 8.9 Hz, 1H, H-5'), 7.18 (m, 1H, H-4''), 7.13 (d, *J* = 3.0 Hz, 1H, H-3'''), 6.70 (d, *J* = 5.6 Hz, 1H, H-6), 6.51 (d, *J* = 3.0 Hz, 1H, H-4'''), 5.23 (s, 2H, OCH₂), 3.82 (s, 2H, CH₂(a)), 3.26 (t, *J* = 6.7 Hz, 2H, CH₂(c)), 3.02 (s, 3H, CH₃), 2.98 (t, *J* = 6.7 Hz, 2H, CH₂(b)). ¹³C NMR (151 MHz, DMSO-*d*₆) δ 163.01, 161.39 (C-3''), 155.96 (C-5'''), 149.26 (C-4'), 145.12 (C-5), 144.66 (C-2'''), 142.29 (C-3a), 142.07 (C-7), 139.76,

139.71 (C-1''), 134.73 (C-1'), 130.58, 130.53 (C-5''), 124.58 (C-7a), 123.39 (C-2'), 123.30 (C-6''), 121.82 (C-3'), 121.38 (C-6'), 115.00 (C-5'), 114.74, 114.60 (C-4''), 114.07, 113.93 (C-2''), 111.24 (C-3'''), 109.25 (C-4'''), 69.51 (OCH₂), 53.63 (CH₂(c)), 45.07 (CH₂(a)), 42.08 (CH₂(b)), 41.46 (CH₃). HR-MS (ESI) *m/z*: calcd for C₂₇H₂₄ClFN₅O₄S, [M-H]⁻ = 568.1216, found 568.1229.

Data for **26**: Yield: 5%. Oil. ¹H NMR (600 MHz, DMSO-*d*₆) δ 7.76 (d, *J* = 2.4 Hz, 1H, H-2'), 7.67 (d, *J* = 5.7 Hz, 1H, H-6), 7.53 – 7.43 (m, 3H, H-5', H-6', H-5''), 7.39 – 7.33 (m, 2H, H-2'', H-6''), 7.22 (m, 1H, H-4''), 6.39 (brs, 2H, NH₂), 6.34 (d, *J* = 3.4 Hz, 1H, H-4'''), 6.29 (d, *J* = 5.7 Hz, 1H, H-7), 6.02 (d, *J* = 3.4 Hz, 1H, H-3'''), 5.36 (s, 2H, OCH₂), 3.69 (s, 2H, CH₂(a)), 3.21 (t, *J* = 6.6 Hz, 2H, CH₂(c)), 2.99 (s, 3H, CH₃), 2.88 (t, *J* = 6.6 Hz, 2H, CH₂(b)). ¹³C NMR (151 MHz, DMSO-*d*₆) δ 163.03, 161.41 (C-3''), 156.03 (C-5'''), 154.25 (C-4'), 152.27 (C-4), 142.83 (C-2'''), 141.60 (C-6), 141.35 (C-7a), 139.12, 139.07 (C-1''), 130.68, 130.63 (C-5''), 129.38 (C-2'), 128.93 (C-1'), 127.99 (C-6'), 125.62 (C-3a), 123.55 (C-6''), 122.28 (C-3'), 114.98, 114.84 (C-4''), 114.90 (C-5'), 114.32, 114.18 (C-2''), 112.50 (C-3'''), 108.90 (C-4'''), 95.87 (C-7), 69.63 (OCH₂), 53.61 (CH₂(c)), 44.88 (CH₂(b)), 42.06 (CH₂(a)), 41.52 (CH₃). HR-MS (ESI) *m/z*: calcd for C₂₇H₂₆ClFN₅O₄S, [M+H]⁺ = 570.1373, found 570.1350.

4.1.12. *2-N-[3-Chloro-4-(3-fluorobenzyloxy)phenyl]-5-fluoro-3-nitropyridine-2,4-diamine (32)*. This compound was prepared using a methodology analogous to that of **7**, starting from the aminopyridine **31** [54] with a slight modification using DMSO as solvent and heating at 150 °C for 24 h. The compound was purified by silica gel column chromatography (cyclohexane/EtOAc: 3/1). Yield: 71%. M.p. = 188-189 °C (EtOAc/*n*-hexane). ¹H NMR (400 MHz, DMSO-*d*₆) δ 10.09 (s, 1H, NH), 8.18 (s, 2H, NH₂), 7.96 (d, *J* = 2.4 Hz, 1H, H-6), 7.84 (d, *J* = 2.6 Hz, 1H, H-2'), 7.44 (m, 2H, H-6', H-5''), 7.29 (m, 2H, H-2'', H-6''), 7.17 (m, 2H, H-5', H-4''), 5.21 (s, 2H, CH₂). ¹³C NMR (151 MHz, DMSO-*d*₆) δ 163.04, 161.42 (C-3''), 149.65 (C-4'), 148.31 (C-2), 143.35, 141.76 (C-5), 142.92, 142.83 (C-4), 139.74, 139.69 (C-1''), 135.35, 135.22 (C-6), 133.06 (C-1'), 130.60, 130.55 (C-5''), 124.28 (C-2'), 123.31 (C-6''), 122.56 (C-6'), 121.12 (C-3'), 116.97 (C-3), 114.76, 114.62 (C-4''), 114.33 (C-5'), 114.07, 113.93 (C-2''), 69.40 (CH₂).

4.1.13. *2-N-[3-Chloro-4-(3-fluorobenzoyloxy)phenyl]-5-fluoropyridine-2,3,4-triamine (33)*. This compound was prepared using a methodology analogous to that of **8**. The compound was purified using silica gel column chromatography (CH₂Cl₂/MeOH: 85/15) and obtained as an oil. Yield: 61%. ¹H NMR (400 MHz, DMSO-*d*₆) δ 7.65 (d, *J* = 2.6 Hz, 1H, H-2'), 7.49 (s, 1H, NH), 7.44 (m, 1H, H-5''), 7.38 (d, *J* = 1.5 Hz, 1H, H-6), 7.29 (m, 2H, H-2'', H-6''), 7.25 (dd, *J* = 9.0, 2.6 Hz, 1H, H-6'), 7.16 (m, 1H, H-4''), 7.06 (d, *J* = 9.0 Hz, 1H, H-5'), 5.38 (s, 2H, 4-NH₂), 5.13 (s, 2H, CH₂), 4.50 (s, 2H, 3-NH₂). ¹³C NMR (151 MHz, DMSO-*d*₆) δ 162.98, 161.37 (C-3''), 146.44, 144.88 (C-5), 146.34 (C-4'), 140.09, 140.04 (C-1''), 139.89 (C-2), 138.09 (C-1'), 130.47, 130.42 (C-5''), 130.12, 130.03 (C-4), 123.28 (C-6''), 121.47 (C-3'), 121.32, 121.18 (C-6), 118.46 (C-2'), 118.09 (C-3), 116.84 (C-6'), 115.32 (C-5'), 114.60, 114.46 (C-4''), 114.03, 113.89 (C-2''), 69.75 (CH₂).

4.1.14. *N-[3-Chloro-4-(3-fluorobenzoyloxy)phenyl]-7-fluoro-2-(furan-2-yl)-1H-imidazo[4,5-*c*]pyridin-4-amine (34)* and *3-[3-chloro-4-(3-fluorobenzoyloxy)phenyl]-6-fluoro-2-(furan-2-yl)-3H-imidazo[4,5-*b*]pyridin-7-amine (35)*. These compounds were prepared using a methodology analogous to that of **9** and **10** respectively and purified by silica gel column chromatography (cyclohexane/ EtOAc: 1/1 to 1/2).

Data for **34**: Yield: 13%. M.p. = 107-108 °C (EtOAc/*n*-hexane). ¹H NMR (600 MHz, DMSO-*d*₆) δ 13.96-13.56 (brs, 1H, imidazole NH), 9.03 (s, 1H, aniline NH), 8.22 (s, 1H, H-2'), 8.00 (s, 1H, H-5'''), 7.86 (d, *J* = 1.4 Hz, 1H, H-6), 7.80-7.70 (brs, 1H, H-6'), 7.46 (m, 1H, H-5''), 7.31 (m, 3H, H-2'', H-6'', H-3'''), 7.17 (m, 2H, H-5', H-4''), 6.77 (dd, *J* = 3.1, 1.5 Hz, 1H, H-4'''), 5.19 (s, 2H, CH₂). ¹³C NMR (151 MHz, DMSO-*d*₆) δ 162.99, 161.38 (C-3''), 147.43 (C-4'), 145.17 (C-5'''), 144.52 (C-2'''), 139.98, 139.93 (C-1''), 135.96 (C-1'), 130.52, 130.46 (C-5''), 124.02, 123.83 (C-6), 123.30 (C-6''), 121.30 (C-3'), 119.80 (C-2'), 118.41 (C-6'), 114.95 (C-5'), 114.65, 114.51 (C-4''), 114.05, 113.91 (C-2''), 112.51 (C-4'''), 111.64 (C-3'''), 69.57 (CH₂). HR-MS (ESI) *m/z*: calcd for C₂₃H₁₄ClF₂N₄O₂, [M-H]⁻ = 451.0768, found 451.0789.

Data for **35**: Yield: 19%, M.p. > 240 °C dec. (Et₂O). ¹H NMR (600 MHz, DMSO-*d*₆) δ 7.91 (d, *J* = 4.0 Hz, 1H, H-5), 7.81 (s, 1H, H-5'''), 7.69 (d, *J* = 2.2 Hz, 1H, H-2'),

7.50 (m, 1H, H-5''), 7.43 (m, 2H, H-5', H-6'), 7.36 (m, 2H, H-2'', H-6''), 7.21 (m, 1H, H-4''), 6.72 (s, 2H, NH₂), 6.56 (dd, $J = 3.3, 1.5$ Hz, 1H, H-4'''), 6.24 (d, $J = 3.3$ Hz, 1H, H-3'''), 5.36 (s, 2H, CH₂). ¹³C NMR (151 MHz, DMSO-*d*₆) δ 163.01, 161.40 (C-3''), 153.88 (C-4'), 146.13 (C-3a), 145.84, 144.30 (C-6), 144.81 (C-5'''), 144.01 (C-2'''), 141.92 (C-2), 139.23, 139.18 (C-1''), 135.08, 134.99 (C-7), 132.05, 131.88 (C-5), 130.66, 130.61 (C-5''), 129.94 (C-2'), 128.51 (C-6'), 128.44 (C-1'), 123.42 (C-6''), 123.20, 123.15 (C-7a), 121.81 (C-3'), 114.91, 114.77 (C-4''), 114.48 (C-5'), 114.21, 114.07 (C-2''), 112.05 (C-3'''), 111.85 (C-4'''), 69.51 (CH₂). HR-MS (ESI) m/z : calcd for C₂₃H₁₄ClF₂N₄O₂, [M-H]⁻ = 451.0768, found 451.0784.

4.1.15. *N*-[3-Chloro-4-(3-fluorobenzoyloxy)phenyl]-7-fluoro-2-{5-[2-(methylsulfonyl)ethylaminomethyl]furan-2-yl}-1*H*-imidazo[4,5-*c*]pyridin-4-amine (36) and 3-[3-chloro-4-(3-fluorobenzoyloxy)phenyl]-6-fluoro-2-{5-[2-(methylsulfonyl)ethylaminomethyl]furan-2-yl}-3*H*-imidazo[4,5-*b*]pyridin-7-amine (37). These compounds were prepared using a methodology analogous to that of **9** and **10** respectively and purified first by silica gel column chromatography (EtOAc/MeOH: 95/5 to 8/2) resulting to a mixture of both products, which were then isolated pure using semi-preparative reverse phase high performance liquid chromatography (H₂O/MeOH: 2/8 to 1/9).

Data for **36**: Yield: 10%. M.p. = 134-135 °C (Et₂O). ¹H NMR (600 MHz, DMSO-*d*₆) δ 13.96 – 13.38 (brs, 1H, imidazole NH), 9.04 (s, 1H, aniline NH), 8.23 (s, 1H, H-2'), 7.86 (d, $J = 0.6$ Hz, 1H, H-6), 7.82 – 7.70 (brs, 1H, H-6'), 7.46 (m, 1H, H-5''), 7.31 (m, 2H, H-2'', H-6''), 7.25 (d, $J = 2.8$ Hz, 1H, H-3'''), 7.16 (m, 2H, H-5', H-4''), 6.57 (d, $J = 2.8$ Hz, 1H, H-4'''), 5.19 (s, 2H, OCH₂), 3.85 (s, 2H, CH₂(a)), 3.27 (t, $J = 6.7$ Hz, 2H, CH₂(c)), 3.02 (s, 3H, CH₃), 2.98 (t, $J = 6.7$ Hz, 2H, CH₂(b)). ¹³C NMR (151 MHz, DMSO-*d*₆) δ 163.06, 161.42 (C-3''), 156.87 (C-5'''), 147.65 (C-4'), 143.61 (C-2'''), 140.17, 140.09 (C-1''), 136.50 (C-1'), 130.65, 130.54 (C-5''), 123.94, 123.87 (C-6), 123.31 (C-6''), 121.28 (C-3'), 120.09 (C-2'), 118.46 (C-6'), 114.82 (C-5'), 114.67, 114.54 (C-4''), 114.07, 113.92 (C-2''), 112.31 (C-3'''), 109.66 (C-4'''), 69.58 (OCH₂), 53.62 (CH₂(c)), 45.11 (CH₂(a)), 42.08 (CH₂(b)), 41.45 (CH₃). HR-MS (ESI) m/z : calcd for C₂₇H₂₃ClF₂N₅O₄S, [M-H]⁻ = 586.1122, found 586.1120.

Data for **37**: Yield: 21%. M.p. = 156-157 °C (Et₂O). ¹H NMR (600 MHz, DMSO-*d*₆) δ 7.89 (d, *J* = 4.1 Hz, 1H, H-5), 7.69 (d, *J* = 2.2 Hz, 1H, H-2'), 7.50 (m, 1H, H-5''), 7.43 (m, 2H, H-5', H-6'), 7.36 (m, 2H, H-2'', H-6''), 7.21 (m, 1H, H-4''), 6.71 (s, 2H, NH₂), 6.35 (d, *J* = 3.4 Hz, 1H, H-4'''), 6.03 (d, *J* = 3.4 Hz, 1H, H-3'''), 5.37 (s, 2H, CH₂), 3.70 (s, 2H, CH₂(a)), 3.22 (t, *J* = 6.7 Hz, 2H, CH₂(c)), 3.00 (s, 3H, CH₃), 2.89 (t, *J* = 6.7 Hz, 2H, CH₂(b)). ¹³C NMR (151 MHz, DMSO-*d*₆) δ 163.03, 161.42 (C-3''), 156.22 (C-5'''), 153.94 (C-4'), 146.21 (C-3a), 145.88, 144.34 (C-6), 142.89 (C-2'''), 142.00 (C-2), 139.24, 139.19 (C-1'), 135.04, 134.94 (C-7), 131.90, 131.76 (C-5), 130.68, 130.63 (C-5''), 130.06 (C-2'), 128.64 (C-6'), 128.45 (C-1'), 123.44 (C-6''), 123.20, 123.15 (C-7a), 121.89 (C-3'), 114.93, 114.79 (C-4''), 114.58 (C-5'), 114.22, 114.07 (C-2''), 112.79 (C-3'''), 108.98 (C-4'''), 69.52 (CH₂), 53.61 (CH₂(c)), 44.90 (CH₂(a)), 42.05 (CH₂(b)), 41.50 (CH₃). HR-MS (ESI) *m/z*: calcd for C₂₇H₂₃ClF₂N₅O₄S, [M-H]⁻ = 586.1122, found 586.1131.

4.1.16. 4-*N*-[3-Chloro-4-(3-fluorobenzyloxy)phenyl]pyrimidine-4,5,6-triamine (**40**) and 4-*N*,6-*N*-bis[3-Chloro-4-(3-fluorobenzyloxy)phenyl]pyrimidine-4,5,6-triamine (**42**). To a solution of the dichloropyrimidine **38** (110 mg, 0.57 mmol) in absolute ethanol (10 mL) were added sodium bicarbonate (65 mg, 0.77 mmol) and a suspension of the aniline **6** (150 mg, 0.60 mmol) in absolute ethanol (5.0 mL) and the mixture was heated at 70 °C for 1 h. Then, a solution of ammonia in absolute ethanol (4 M, 3.0 mL) was added dropwise and heating was continued at 70 °C for 2 h. The solvent was vacuum-evaporated, water was added to the residue and the precipitate was filtered, washed with water and dried. A small amount of the crude mixture was purified using preparative thin layer chromatography (cyclohexane/EtOAc: 1/1) in order to isolate and identify intermediates **39** and **41**. The remaining mixture of the nitroderivatives was submitted to reduction according to the synthetic procedure described for compound **8**. The reduced products were separated by silica gel column chromatography (CH₂Cl₂/MeOH: 97/3 to 8/2).

Data for 4-*N*-[3-Chloro-4-(3-fluorobenzyloxy)phenyl]-5-nitropyrimidine-4,6-diamine (**39**): M.p. = 230-231 °C (Et₂O). ¹H NMR (600 MHz, DMSO-*d*₆) δ 10.69 (s, 1H, NH), 8.63 (s, 2H, NH₂), 8.01 (s, 1H, H-2), 7.77 (d, *J* = 2.6 Hz, 1H, H-2'), 7.47 (m, 1H, H-5''), 7.44 (dd, *J* = 9.0, 2.6 Hz, 1H, H-6'), 7.30 (m, 2H, H-2'', H-6''), 7.22 (d, *J* = 9.0

Hz, 1H, H-5'), 7.17 (m, 1H, H-4''), 5.25 (s, 2H, CH₂). ¹³C NMR (151 MHz, DMSO-*d*₆) δ 163.02, 161.40 (C-3''), 159.33 (C-2), 158.71 (C-6), 155.43 (C-4), 150.84 (C-4'), 139.59, 139.54 (C-1''), 131.35 (C-1'), 130.63, 130.57 (C-5''), 126.25 (C-2'), 124.48 (C-6'), 123.32 (C-6''), 121.00 (C-3'), 114.80, 114.66 (C-4''), 114.08, 113.94 (C-2''), 114.05 (C-5'), 112.13 (C-5), 69.33 (CH₂).

Data for 4-*N*,6-*N*-bis[3-Chloro-4-(3-fluorobenzyloxy)phenyl]-5-nitropyrimidine-4,6-diamine (**41**): M.p. > 220 °C dec. (Et₂O). ¹H NMR (600 MHz, DMSO-*d*₆) δ 10.75 (s, 2H, NH), 8.12 (s, 1H, H-2), 7.74 (d, *J* = 2.4 Hz, 2H, H-2'), 7.47 (m, 2H, H-5''), 7.44 (dd, *J* = 9.0, 2.4 Hz, 2H, H-6'), 7.33 – 7.28 (m, 4H, H-2'', H-6''), 7.24 (d, *J* = 9.0 Hz, 2H, H-5'), 7.18 (m, 2H, H-4''), 5.26 (s, 4H, CH₂). ¹³C NMR (151 MHz, DMSO-*d*₆) δ 163.01, 161.40 (C-3''), 159.06 (C-2), 155.47 (C-4, C-6), 151.10 (C-4'), 139.54, 139.49 (C-1''), 131.18 (C-1'), 130.60, 130.54 (C-5''), 126.48 (C-2'), 124.75 (C-6'), 123.27 (C-6''), 121.10 (C-3'), 114.77, 114.63 (C-4''), 114.14 (C-5'), 114.04, 113.90 (C-2''), 112.95 (C-5), 69.43 (CH₂).

Data for **40**: 90 mg, Total yield of 3 steps: 44%. Oil. ¹H NMR (600 MHz, DMSO-*d*₆) δ 8.07 (s, 1H, NH), 7.79 (d, *J* = 2.6 Hz, 1H, H-2'), 7.74 (s, 1H, H-2), 7.45 (m, 1H, H-5''), 7.42 (dd, *J* = 9.0, 2.6 Hz, 1H, H-6'), 7.29 (m, 2H, H-2'', H-6''), 7.16 (m, 1H, H-4''), 7.14 (d, *J* = 9.0 Hz, 1H, H-5'), 6.21 (s, 2H, 6-NH₂), 5.18 (s, 2H, CH₂), 4.31 (s, 2H, 5-NH₂). ¹³C NMR (151 MHz, DMSO-*d*₆) δ 163.06, 161.45 (C-3''), 151.59 (C-6), 147.99 (C-4'), 147.01 (C-4), 146.39 (C-2), 139.95, 139.90 (C-1''), 135.44 (C-1'), 130.61, 130.56 (C-5''), 123.37 (C-6''), 121.33 (C-3'), 121.26 (C-2'), 119.46 (C-6'), 114.91 (C-5'), 114.75, 114.61 (C-4''), 114.11, 113.97 (C-2''), 108.65 (C-5), 69.62 (CH₂).

Data for **42**: 10 mg, Total yield of 3 steps: 3.5%. Oil. ¹H NMR (600 MHz, DMSO-*d*₆) δ 8.11 (s, 2H, NH), 7.91 (s, 1H, H-2), 7.88 (d, *J* = 2.6 Hz, 2H, H-2'), 7.48 (dd, *J* = 9.1, 2.6 Hz, 2H, H-6'), 7.45 (m, 2H, H-5''), 7.33 – 7.28 (m, 4H, H-2'', H-6''), 7.17 (m, 2H, H-4''), 7.15 (d, *J* = 9.1 Hz, 2H, H-5'), 5.19 (s, 4H, CH₂), 4.54 (s, 2H, NH₂). ¹³C NMR (151 MHz, DMSO-*d*₆) δ 163.03, 161.42 (C-3''), 147.90 (C-4, C-6), 147.83 (C-4'), 146.17 (C-2), 139.93, 139.88 (C-1''), 135.61 (C-1'), 130.56, 130.50 (C-5''), 123.32 (C-6''), 121.31 (C-3'), 121.00 (C-2'), 119.20 (C-6'), 114.89 (C-5'), 114.70, 114.57 (C-4''), 114.08, 113.94 (C-2''), 110.24 (C-5), 69.59 (CH₂).

4.1.17. 6-*N*-[3-Chloro-4-(3-fluorobenzyloxy)phenyl]-8-(furan-2-yl)-9*H*-purin-6-amine (**43**) and 9-[3-chloro-4-(3-fluorobenzyloxy)phenyl]-8-(furan-2-yl)-9*H*-purin-6-amine (**44**). These compounds were prepared using a methodology analogous to that of **9** and **10** respectively and purified first by silica gel column chromatography (CH₂Cl₂/MeOH: 95/5 to 9/1) resulting to a mixture of both products, which were then isolated pure using preparative thin layer chromatography (CH₂Cl₂/MeOH: 95/5).

Data for **43**: Yield: 10%. M.p. > 250 °C dec. (MeOH). ¹H NMR (600 MHz, DMSO-*d*₆) δ 13.88 – 13.13 (brs, 1H, imidazole NH), 9.88 (s, 1H, aniline NH), 8.37 (s, 1H, H-2), 8.21 (d, *J* = 2.1 Hz, 1H, H-2'), 7.95 (d, *J* = 1.2 Hz, 1H, H-5'''), 7.82 (dd, *J* = 8.9, 2.1 Hz, 1H, H-6'), 7.46 (m, 1H, H-5''), 7.31 (m, 2H, H-2'', H-6''), 7.23 (d, *J* = 3.3 Hz, 1H, H-3'''), 7.20 (d, *J* = 8.9 Hz, 1H, H-5'), 7.17 (m, 1H, H-4''), 6.74 (dd, *J* = 3.3, 1.2 Hz, 1H, H-4'''), 5.22 (s, 2H, CH₂). ¹³C NMR (151 MHz, DMSO-*d*₆) δ 163.02, 161.41 (C-3''), 151.95 (C-2), 148.67 (C-4'), 145.09 (C-5'''), 144.91 (C-2'''), 139.84, 139.80 (C-1''), 134.18 (C-1'), 130.58, 130.53 (C-5''), 123.32 (C-6''), 122.04 (C-2'), 121.13 (C-3'), 120.33 (C-6'), 114.73, 114.59 (C-4''), 114.59 (C-5'), 114.08, 113.94 (C-2''), 112.39 (C-4'''), 111.30 (C-3'''), 69.46 (CH₂). HR-MS (ESI) *m/z*: calcd for C₂₂H₁₄ClFN₅O₂, [M-H]⁻ = 434.0815, found 434.0834.

Data for **44**: Yield: 10%. M.p. = 232-233 °C (Et₂O). ¹H NMR (600 MHz, DMSO-*d*₆) δ 8.07 (s, 1H, H-2), 7.82 (d, *J* = 1.5 Hz, 1H, H-5'''), 7.74 (d, *J* = 2.5 Hz, 1H, H-2'), 7.49 (m, 4H, NH₂, H-6', H-5''), 7.42 (d, *J* = 8.8 Hz, 1H, H-5'), 7.36 (m, 2H, H-2'', H-6''), 7.22 (m, 1H, H-4''), 6.56 (dd, *J* = 3.5, 1.5 Hz, 1H, H-4'''), 6.21 (d, *J* = 3.5 Hz, 1H, H-3'''), 5.37 (s, 2H, CH₂). ¹³C NMR (151 MHz, DMSO-*d*₆) δ 163.03, 161.41 (C-3''), 155.85 (C-6), 154.06 (C-4'), 153.23 (C-2), 151.95 (C-4), 144.88 (C-5'''), 143.85 (C-2'''), 140.57 (C-8), 139.21, 139.16 (C-1''), 130.69, 130.64 (C-5''), 129.80 (C-2'), 128.37 (C-6'), 128.06 (C-1'), 123.46 (C-6''), 121.85 (C-3'), 118.30 (C-5), 114.95, 114.81 (C-4''), 114.50 (C-5'), 114.25, 114.10 (C-2''), 112.10 (C-3'''), 111.88 (C-4'''), 69.53 (CH₂). HR-MS (ESI) *m/z*: calcd for C₂₂H₁₆ClFN₅O₂, [M+H]⁺ = 436.0971, found 436.0967.

4.1.18. 6-*N*-[3-Chloro-4-(3-fluorobenzyloxy)phenyl]-8-{5-[2-(methylsulfonyl)ethylaminomethyl]furan-2-yl}-9*H*-purin-6-amine (**45**) and 9-[3-chloro-4-(3-fluorobenzyloxy)phenyl]-8-{5-[2-

(methylsulfonyl)ethylaminomethyl]furan-2-yl]-9H-purin-6-amine (**46**). These compounds were prepared using a methodology analogous to that of **9** and **10** respectively and purified first by silica gel column chromatography (CH₂Cl₂/MeOH: 95/5 to 8/2) resulting to a mixture of both products, which were then isolated pure using preparative thin layer chromatography (EtOAc/Me₂CO: 2/8).

Data for **45**: Yield: 10%. M.p. = 238-239 °C (Et₂O). ¹H NMR (600 MHz, DMSO-*d*₆) δ 13.78 – 12.98 (brs, 1H, imidazole NH), 9.88 (s, 1H, aniline NH), 8.36 (s, 1H, H-2), 8.22 (d, *J* = 2.2 Hz, 1H, H-2'), 7.83 (d, *J* = 7.8 Hz, 1H, H-6'), 7.46 (m, 1H, H-5''), 7.31 (m, 2H, H-2'', H-6''), 7.18 (m, 3H, H-5', H-4'', H-3'''), 6.54 (d, *J* = 2.9 Hz, 1H, H-4'''), 5.22 (s, 2H, OCH₂), 3.83 (s, 2H, CH₂(a)), 3.27 (t, *J* = 6.7 Hz, 2H, CH₂(c)), 3.02 (s, 3H, CH₃), 2.97 (t, *J* = 6.7 Hz, 2H, CH₂(b)). ¹³C NMR (151 MHz, DMSO-*d*₆) δ 163.00, 161.38 (C-3''), 156.45 (C-5'''), 151.79 (C-2), 148.59 (C-4'), 143.90 (C-2'''), 139.83, 139.78 (C-1''), 134.24 (C-1'), 130.55, 130.49 (C-5'), 123.29 (C-6''), 122.03 (C-2'), 121.09 (C-3'), 120.27 (C-6'), 114.70, 114.56 (C-4''), 114.56 (C-5'), 114.06, 113.91 (C-2''), 112.09 (C-3'''), 109.43 (C-4'''), 69.43 (OCH₂), 53.62 (CH₂(c)), 45.06 (CH₂(a)), 42.06 (CH₂(b)), 41.45 (CH₃). HR-MS (ESI) *m/z*: calcd for C₂₆H₂₃ClFN₆O₄S, [M-H]⁻ = 569.1169, found 569.1183.

Data for **46**: Yield: 20%. M.p. 204-205 °C (Et₂O). ¹H NMR (600 MHz, DMSO-*d*₆) δ 8.07 (s, 1H, H-2), 7.73 (d, *J* = 2.2 Hz, 1H, H-2'), 7.53 – 7.41 (m, 5H, NH₂, H-5', H-6', H-5''), 7.35 (m, 2H, H-2'', H-6''), 7.21 (m, 1H, H-4''), 6.35 (d, *J* = 3.4 Hz, 1H, H-4'''), 6.02 (d, *J* = 3.4 Hz, 1H, H-3'''), 5.37 (s, 2H, OCH₂), 3.70 (s, 2H, CH₂(a)), 3.22 (t, *J* = 6.6 Hz, 2H, CH₂(c)), 2.99 (s, 3H, CH₃), 2.88 (t, *J* = 6.6 Hz, 2H, CH₂(b)). ¹³C NMR (151 MHz, DMSO-*d*₆) δ 163.02, 161.40 (C-3''), 156.24 (C-5'''), 155.77 (C-6), 154.11 (C-4'), 153.10 (C-2), 152.00 (C-4), 142.72 (C-2'''), 140.62 (C-8), 139.19, 139.14 (C-1''), 130.67, 130.62 (C-5'), 129.87 (C-2'), 128.46 (C-6''), 128.04 (C-1'), 123.43 (C-6''), 121.92 (C-3'), 118.28 (C-5), 114.93, 114.79 (C-4''), 114.58 (C-5'), 114.22, 114.07 (C-2''), 112.80 (C-3'''), 108.96 (C-4'''), 69.54 (OCH₂), 53.60 (CH₂(c)), 44.88 (CH₂(a)), 42.03 (CH₂(b)), 41.50 (CH₃). HR-MS (ESI) *m/z*: calcd for C₂₆H₂₃ClFN₆O₄S, [M-H]⁻ = 569.1169, found 569.1190.

4.2 Docking calculations

Rigid docking was performed with the Glide SP algorithm and a scaling factor of 0.8 was utilized for both the protein and ligand atoms to account for possible induced-fit effects upon inhibitor binding. The best poses were re-docked and the ligand binding affinities were subsequently evaluated by using the EMBRACE module of Maestro with the energy difference option, using the OPLS-2005 force field and the generalized Born model for water while protein flexibility was permitted in a radius of 6 Å around the binding pocket.

4.3 Biological evaluation

4.3.1. Cell Cultures

The EGFR positive NSCLC cell lines A549 and NCI-H1975 and breast cancer cell lines HCC-1954 and MCF-7 used in this study were tested for mycoplasma contamination on a regular basis using the MycoAlert™ Mycoplasma Detection Kit (Lonza, USA). Cells were maintained in DMEM and RPMI (Roswell Park Memorial Institute) medium, containing glutamine and supplemented with 10% fetal bovine serum (FBS), penicillin (100 U/mL), and streptomycin (100 mg/mL) at 37 °C and 5% CO₂. Lapatinib was purchased from MedChem Express (Sollentuna Sweden).

4.3.2. Biochemical Tyrosine Kinase Assay

The trans-phosphorylation activity of EGFR and HER2 was evaluated as described before [58]. Briefly, reactions were performed in 96-well microtiter plates precoated (20 µg/well in PBS; incubated overnight at 4 °C) with the peptide substrate poly-Glu,Tyr (4:1). Excess protein binding sites were blocked with the addition of 5% (w/v) BSA in PBS. Purified GST-fusion proteins were then added to the microtiter wells in 2 × concentration kinase dilution buffer consisting of 100 mM HEPES, 50 mM NaCl, 40 µM NaVO₄, and 0.02% (w/v) BSA. The final enzyme concentration for each GST-kinase was 200 ng/mL (**Table S3**). 25 µL of diluted lapatinib or each of the new derivatives were subsequently added to each reaction well to produce a range of inhibitor concentrations (1-10 µM) appropriate for each enzyme. The kinase reaction was initiated by the addition of different concentrations of ATP in a solution of MnCl₂

so that the final ATP concentrations spanned the K_m for the enzyme, and the final concentration of $MnCl_2$ was 10 mM. The plates were incubated for 60 minutes at 37 °C before stopping the reaction with the addition of EDTA. The plates were then washed three times with TBST. Rabbit polyclonal antiphosphotyrosine antisera conjugated to HRP was added to the wells at a 2:1000 dilution in TBST containing 0.75% (w/v) BSA, 0.025% (w/v) nonfat dry milk, and 100 μM $NaVO_4$ and incubated for one hour at 37 °C. The plates were then washed three times with TBST and the amount of phosphotyrosine in each well was quantified after the addition of 2,2'-azino-di-[3-ethylbenzthiazoline sulfonate] substrate (A1888, Sigma-Aldrich, Munich, Germany) and measured at 405 nm. Each experiment was performed in triplicate.

4.3.3. Cellular Kinase Assay based on Western Blot Analysis

A549 cells (for EGFR) and HCC-1954 (for HER2) were used in studies of inhibition of autophosphorylation. A549 cells were plated in 6-well plates and when grown at 60-70% confluence they were serum starved for 24 h. Serum starved cells were treated with lapatinib (0.01 μM and 1 μM) or with the tested compounds (1 μM and 10 μM) for 10 min and then stimulated with 100 ng/mL EGF for another 10 min at 37°C. After 10 min incubation, the cell medium was removed and the cells were lysed in RIPA lysis buffer (50 mM Tris-HCl at pH 7.5, 150 mM NaCl, 5 mM Na_2EDTA , 1mM EGTA, 0.1% SDS, 1% NP-40, 0.5 % sodium deoxycholate, 8mM sodium fluoride and 1mM sodium orthovanadate) and Protease Inhibitor Cocktail (Roche, UK). HCC-1954 cells were plated in 6-well plates and when grown at 60-70% confluence were treated with lapatinib or the examined derivatives (0.02 μM and 2 μM) for 1 h. After 1h incubation, cells were lysed with RIPA lysis buffer as mentioned above.

Protein concentration was determined using the Pierce BCA assay kit (Pierce, Rockford, IL, USA) according to the manufacturer's specifications. Protein isolated from A549 and HCC-1954 cell lysate (approximately 10 μg of protein/cell line), along with NuPAGE Sample Reducing agent and NuPAGE LDS Sample Buffer (both from Invitrogen, UK) were separated by SDS page and transferred to polyvinylidene difluoride (PVDF) membranes. The membranes were then blocked in 5% non-fat dry milk in TBS-T buffer for 1 h at room temperature.

Phosphorylated and total EGFR and HER2 were detected using specific antibodies at 1:1000 dilution in TBST (**Table S4**). This process was followed by another incubation for 1 h at room temperature with the secondary anti-rabbit peroxidase-conjugated antibody and anti-mouse peroxidase-conjugated antibody (Cell Signalling, UK) at a 1:1000 dilution, followed by Enhanced Chemiluminescence (GE Healthcare, UK) visualization. For normalization of protein concentration, the rabbit monoclonal antibody b-actin (Abcam, UK) was used.

4.3.4. *In Vitro* Cytotoxicity Assay

Cells were plated in complete growth medium in 96-well plates at a density of 5×10^3 cells per well. After 24 h incubation (37°C, 5% CO₂), the cell medium was removed, and compounds were added at various concentrations (0.5–150 µM), followed by incubation for 72 h.

The medium was then removed and the MTT solution (0.3 mg/mL in PBS) was added to cells for 3 h, after which the MTT solution was removed and the formazan crystals were dissolved in 100 µL DMSO. The optical density was measured at 570 nm and a reference wavelength of 650 nm using an absorbance microplate reader (SpectraMax 190, Molecular Devices, Sunnyvale, CA, USA). The 50% cytostatic concentration (IC₅₀) was calculated based on a four-parameter logistic equation using SigmaPlot 12.5 software (Systat Software, SanJose, CA, USA). Each point was the result of three experiments performed in triplicate.

4.3.5. *Characterization and Quantification of Lapatinib, 23 and 45 Using LC-MS/MS Analysis*

For the identification and quantification of lapatinib, **23** and **45** LC-MS/MS methodologies were developed. HPLC was performed using a Dionex Ultimate 3000 system (Dionex Corporation, Germering, Germany) equipped with three pumps (two for nano and one for microLC), a temperature controlled column compartment, and an autosampler. A dC18 column (Water, Atlantis, 2.1 × 50 mm, 3 µM) was used at a flow rate of 300 µL/min for the separation of analytes of interest. The mobile phase consisted of A: 10% ACN, 90% water, 2 mM ammonium acetate, and 0.1% FA and B: 90% ACN, 10% water, 2 mM ammonium acetate, and 0.1% FA. Mass

spectrometry was performed on an API 4000 QTRAP LC-MS/MS system fitted with a Turbo Ion Spray source and a hybrid triple quadrupole/linear ion trap mass spectrometer (Applied Biosystems, Concord, Ontario, Canada).

4.3.6. Polar Surface Area and *cLogP* Predictions

Total polar surface area and *clogP* values, were predicted by Chemdraw Ultra (v10, PerkinElmer Informatics, USA).

4.3.7. Cellular Uptake of Lapatinib, **23** and **45** using LC-MS/MS Analysis

The cellular uptake assay was performed as described before [59, 60]. Briefly A549 cells were plated in 6-well plates at a density of 1.5×10^5 cells/well. Cells were incubated with lapatinib, **23** or **45** (1 μ M) for selected time points (1 h, 4 h, 8 h, 24 h, 48 h). Incubations were terminated by removing the medium and washing the cells twice with ice-cold PBS to remove unbound lapatinib, **23** or **45**. The cells were then lysed by adding an ice-cold solution of ACN–Water (3:2) and scraping the cell monolayer. Cell lysates were subsequently vortexed, sonicated, and centrifuged for three minutes at 16,060 g (Heraeus Biofuge Pico microcentrifuge, Thermo Scientific, Bonn, Germany). The supernatants were collected, evaporated, and stored at -20 °C until the day of analysis. The intracellular levels of lapatinib, **23** and **45** were measured by LC-MS/MS analysis using lapatinib, **23** and **45** standards and a stable internal standard for the construction of analytical standard curves.

4.3.8. Pharmacokinetic Study in Mice

All animal procedures were approved by the Project Evaluation Committee of the Institution and the competent Veterinary Service of the Prefecture of Athens, in accordance to the National legal framework on the protection of animals used for scientific purposes (Presidential Decree 56/2013 in harmonization to the European Directive 2010/63). For the pharmacokinetic studies, animals at the age of 10–12 weeks were weighed and fasted overnight before dosing (n = 5 per group, male

C57BL/6N inbred strain obtained from Charles River, Calco, Italy). Equimolar (3.4×10^3 nmol/Kg) dosing solutions for each compound (lapatinib, **23** and **45**) were prepared in 0.5% carboxymethyl cellulose: 0.1% Tween 80 in water and administered via oral gavage.

A serial tail bleeding protocol was used for the collection of blood samples as described before [58, 59, 61]. Blood samples (10 μ L) were collected at selected time points (0.25 h, 0.5 h, 1 h, 2 h, 4 h, 6 h, 8 h, 24 h) in tubes containing 40 μ L citric acid (0.1 M, pH 4.5) and stored at -80 °C until sample extraction. Samples were prepared for quantification by protein precipitation and evaporation. Lapatinib, **23** and **45** levels in blood were measured by LC-MS/MS analysis.

4.3.9. *In vivo* efficacy of lapatinib and **23**

NOD/SCID (Non-Obese Diabetic/Severe Combined ImmunoDeficient) mice (n=4 per group, consisting of 2 male and 2 female) were injected in each flank with 5×10^6 A549 cells in DMEM medium, 10% FBS. Pharmacological treatment was initiated when tumors reached 160 mm^3 by daily oral administrations of lapatinib or equimolar dose of **23** (86 μ mol/Kg). Control mice received 0.5% Carboxymethyl cellulose: 0.1% Tween 80 in water. Mice were weighed regularly and phenotypic signs of discomfort were monitored. Tumor growth was monitored every three days by caliper measurements and volumes were calculated based on the formula: $V = \pi \times D \times d^2/6$ (D and d represent the larger and smaller diameters of the tumors, respectively). The experiment was terminated after 27 days, at 2h after the last administered dose by euthanizing the animals under isoflurane anaesthesia. Tumors were excised, weighed and prepared for quantification by LC-MS/MS.

4.4. *Statistical analysis*

The results presented herein are expressed as mean \pm SD. Statistical analyses and calculation of all IC_{50} 's were performed by SigmaPlot 12.5 software and statistical significance was determined using the Student's t-test.

5. Conflict of interest disclosure

The authors declare that they have no conflict of interest to disclosure.

6. Authors declaration

All authors have participated significantly in the completion of the manuscript. ESG, AD, EM, PM, CT, NP: conceived and designed the experiments; ESG, AD, VM, SD performed the experiments; ESG, AD, TK, VM, EM, PM, CT, NP: analysed the data; ESG, AD, EM, PM, CT, NP: wrote the manuscript.

Acknowledgments

Aris Doukatas was funded by State Scholarships Foundation (IKY), financed by the European Union (European Social Fund - ESF) and Greek national funds through the actions entitle “Reinforcement of Doctoral Researchers”, in the framework of the Operational Programme “Human Resources Development Program, Education and Lifelong Learning” of the National Strategic Reference Framework (NSRF) 2014 – 2020.

References

- [1] M.A. Lemmon, J. Schlessinger, Cell signaling by receptor tyrosine kinases, *Cell*, 141 (2010) 1117-1134.
- [2] R. Roskoski, Jr., The ErbB/HER family of protein-tyrosine kinases and cancer, *Pharmacological research*, 79 (2014) 34-74.
- [3] A. Ullrich, L. Coussens, J.S. Hayflick, T.J. Dull, A. Gray, A.W. Tam, J. Lee, Y. Yarden, T.A. Libermann, J. Schlessinger, et al., Human epidermal growth factor receptor cDNA sequence and aberrant expression of the amplified gene in A431 epidermoid carcinoma cells, *Nature*, 309 (1984) 418-425.
- [4] H. Ogiso, R. Ishitani, O. Nureki, S. Fukai, M. Yamanaka, J.H. Kim, K. Saito, A. Sakamoto, M. Inoue, M. Shirouzu, S. Yokoyama, Crystal structure of the complex of human epidermal growth factor and receptor extracellular domains, *Cell*, 110 (2002) 775-787.
- [5] N. Normanno, A. De Luca, C. Bianco, L. Strizzi, M. Mancino, M.R. Maiello, A. Carotenuto, G. De Feo, F. Caponigro, D.S. Salomon, Epidermal growth factor receptor (EGFR) signaling in cancer, *Gene*, 366 (2006) 2-16.

- [6] S. Sebastian, J. Settleman, S.J. Reshkin, A. Azzariti, A. Bellizzi, A. Paradiso, The complexity of targeting EGFR signalling in cancer: from expression to turnover, *Biochimica et biophysica acta*, 1766 (2006) 120-139.
- [7] Y. Yarden, M.X. Sliwkowski, Untangling the ErbB signalling network, *Nature reviews. Molecular cell biology*, 2 (2001) 127-137.
- [8] N.E. Hynes, H.A. Lane, ERBB receptors and cancer: the complexity of targeted inhibitors, *Nature reviews. Cancer*, 5 (2005) 341-354.
- [9] G. Pines, W.J. Kostler, Y. Yarden, Oncogenic mutant forms of EGFR: lessons in signal transduction and targets for cancer therapy, *FEBS letters*, 584 (2010) 2699-2706.
- [10] K.S. Gajiwala, J. Feng, R. Ferre, K. Ryan, O. Brodsky, S. Weinrich, J.C. Kath, A. Stewart, Insights into the aberrant activity of mutant EGFR kinase domain and drug recognition, *Structure*, 21 (2013) 209-219.
- [11] D. Ayeni, K. Politi, S.B. Goldberg, Emerging Agents and New Mutations in EGFR-Mutant Lung Cancer, *Clinical cancer research : an official journal of the American Association for Cancer Research*, 21 (2015) 3818-3820.
- [12] S. Sharpe, K.R. Barber, C.W. Grant, Val(659)-->Glu mutation within the transmembrane domain of ErbB-2: effects measured by ²H NMR in fluid phospholipid bilayers, *Biochemistry*, 39 (2000) 6572-6580.
- [13] G. Li, X. Wang, H. Hibshoosh, C. Jin, B. Halmos, Modulation of ErbB2 blockade in ErbB2-positive cancers: the role of ErbB2 Mutations and PHLDA1, *PloS one*, 9 (2014) e106349.
- [14] B.S. Jaiswal, N.M. Kljavin, E.W. Stawiski, E. Chan, C. Parikh, S. Durinck, S. Chaudhuri, K. Pujara, J. Guillory, K.A. Edgar, V. Janakiraman, R.P. Scholz, K.K. Bowman, M. Lorenzo, H. Li, J. Wu, W. Yuan, B.A. Peters, Z. Kan, J. Stinson, M. Mak, Z. Modrusan, C. Eigenbrot, R. Firestein, H.M. Stern, K. Rajalingam, G. Schaefer, M.A. Merchant, M.X. Sliwkowski, F.J. de Sauvage, S. Seshagiri, Oncogenic ERBB3 mutations in human cancers, *Cancer cell*, 23 (2013) 603-617.
- [15] K.J. Kurppa, K. Denessiouk, M.S. Johnson, K. Elenius, Activating ERBB4 mutations in non-small cell lung cancer, *Oncogene*, 35 (2016) 1283-1291.
- [16] C. Lau, K.J. Killian, Y. Samuels, U. Rudloff, ERBB4 mutation analysis: emerging molecular target for melanoma treatment, *Methods in molecular biology*, 1102 (2014) 461-480.
- [17] H.S. Cho, K. Mason, K.X. Ramyar, A.M. Stanley, S.B. Gabelli, D.W. Denney, Jr., D.J. Leahy, Structure of the extracellular region of HER2 alone and in complex with the Herceptin Fab, *Nature*, 421 (2003) 756-760.
- [18] E.A. Sickmier, R.J. Kurzeja, K. Michelsen, M. Vazir, E. Yang, A.S. Tasker, The Panitumumab EGFR Complex Reveals a Binding Mechanism That Overcomes Cetuximab Induced Resistance, *PloS one*, 11 (2016) e0163366.
- [19] M.C. Franklin, K.D. Carey, F.F. Vajdos, D.J. Leahy, A.M. de Vos, M.X. Sliwkowski, Insights into ErbB signaling from the structure of the ErbB2-pertuzumab complex, *Cancer cell*, 5 (2004) 317-328.
- [20] P.M. LoRusso, D. Weiss, E. Guardino, S. Girish, M.X. Sliwkowski, Trastuzumab emtansine: a unique antibody-drug conjugate in development for human epidermal growth factor receptor 2-positive cancer, *Clinical cancer research : an official journal of the American Association for Cancer Research*, 17 (2011) 6437-6447.
- [21] S. Li, K.R. Schmitz, P.D. Jeffrey, J.J. Wiltzius, P. Kussie, K.M. Ferguson, Structural basis for inhibition of the epidermal growth factor receptor by cetuximab, *Cancer cell*, 7 (2005) 301-311.
- [22] M.H. Cohen, G.A. Williams, R. Sridhara, G. Chen, W.D. McGuinn, Jr., D. Morse, S. Abraham, A. Rahman, C. Liang, R. Lostritto, A. Baird, R. Pazdur, United States Food and Drug Administration Drug Approval summary: Gefitinib (ZD1839; Iressa) tablets, *Clinical cancer research : an official journal of the American Association for Cancer Research*, 10 (2004) 1212-1218.

- [23] M.H. Cohen, J.R. Johnson, Y.F. Chen, R. Sridhara, R. Pazdur, FDA drug approval summary: erlotinib (Tarceva) tablets, *The oncologist*, 10 (2005) 461-466.
- [24] P.J. Medina, S. Goodin, Lapatinib: a dual inhibitor of human epidermal growth factor receptor tyrosine kinases, *Clinical therapeutics*, 30 (2008) 1426-1447.
- [25] D. Viola, L. Valerio, E. Molinaro, L. Agate, V. Bottici, A. Biagini, L. Lorusso, V. Cappagli, L. Pieruzzi, C. Giani, E. Sabini, P. Passannati, L. Puleo, A. Matrone, B. Pontillo-Contillo, V. Battaglia, S. Mazzeo, P. Vitti, R. Elisei, Treatment of advanced thyroid cancer with targeted therapies: ten years of experience, *Endocrine-related cancer*, 23 (2016) R185-205.
- [26] G.M. Keating, Afatinib: a review of its use in the treatment of advanced non-small cell lung cancer, *Drugs*, 74 (2014) 207-221.
- [27] A. Yver, Osimertinib (AZD9291)-a science-driven, collaborative approach to rapid drug design and development, *Annals of oncology : official journal of the European Society for Medical Oncology*, 27 (2016) 1165-1170.
- [28] D.R. Camidge, W. Pao, L.V. Sequist, Acquired resistance to TKIs in solid tumours: learning from lung cancer, *Nature reviews. Clinical oncology*, 11 (2014) 473-481.
- [29] D.A. Cross, S.E. Ashton, S. Ghiorghiu, C. Eberlein, C.A. Nebhan, P.J. Spitzler, J.P. Orme, M.R. Finlay, R.A. Ward, M.J. Mellor, G. Hughes, A. Rahi, V.N. Jacobs, M. Red Brewer, E. Ichihara, J. Sun, H. Jin, P. Ballard, K. Al-Kadhimi, R. Rowlinson, T. Klinowska, G.H. Richmond, M. Cantarini, D.W. Kim, M.R. Ranson, W. Pao, AZD9291, an irreversible EGFR TKI, overcomes T790M-mediated resistance to EGFR inhibitors in lung cancer, *Cancer discovery*, 4 (2014) 1046-1061.
- [30] R. Minari, P. Bordi, M. Tiseo, Third-generation epidermal growth factor receptor-tyrosine kinase inhibitors in T790M-positive non-small cell lung cancer: review on emerged mechanisms of resistance, *Translational lung cancer research*, 5 (2016) 695-708.
- [31] H. Patel, R. Pawara, A. Ansari, S. Surana, Recent updates on third generation EGFR inhibitors and emergence of fourth generation EGFR inhibitors to combat C797S resistance, *European journal of medicinal chemistry*, 142 (2017) 32-47.
- [32] S. Wang, Y. Song, D. Liu, EAI045: The fourth-generation EGFR inhibitor overcoming T790M and C797S resistance, *Cancer letters*, 385 (2017) 51-54.
- [33] M. Juchum, M. Gunther, E. Doring, A. Sievers-Engler, M. Lammerhofer, S. Laufer, Trisubstituted Imidazoles with a Rigidized Hinge Binding Motif Act As Single Digit nM Inhibitors of Clinically Relevant EGFR L858R/T790M and L858R/T790M/C797S Mutants: An Example of Target Hopping, *Journal of medicinal chemistry*, 60 (2017) 4636-4656.
- [34] M. Gunther, J. Lategahn, M. Juchum, E. Doring, M. Keul, J. Engel, H.L. Tumbrink, D. Rauh, S. Laufer, Trisubstituted Pyridinylimidazoles as Potent Inhibitors of the Clinically Resistant L858R/T790M/C797S EGFR Mutant: Targeting of Both Hydrophobic Regions and the Phosphate Binding Site, *Journal of medicinal chemistry*, 60 (2017) 5613-5637.
- [35] D.W. Rusnak, K. Lackey, K. Affleck, E.R. Wood, K.J. Alligood, N. Rhodes, B.R. Keith, D.M. Murray, W.B. Knight, R.J. Mullin, T.M. Gilmer, The effects of the novel, reversible epidermal growth factor receptor/ErbB-2 tyrosine kinase inhibitor, GW2016, on the growth of human normal and tumor-derived cell lines in vitro and in vivo, *Molecular cancer therapeutics*, 1 (2001) 85-94.
- [36] D.W. Rusnak, K. Affleck, S.G. Cockerill, C. Stubberfield, R. Harris, M. Page, K.J. Smith, S.B. Guntrip, M.C. Carter, R.J. Shaw, A. Jowett, J. Stables, P. Topley, E.R. Wood, P.S. Brignola, S.H. Kadwell, B.R. Reep, R.J. Mullin, K.J. Alligood, B.R. Keith, R.M. Crosby, D.M. Murray, W.B. Knight, T.M. Gilmer, K. Lackey, The characterization of novel, dual ErbB-2/EGFR, tyrosine kinase inhibitors: potential therapy for cancer, *Cancer research*, 61 (2001) 7196-7203.
- [37] S. Cockerill, C. Stubberfield, J. Stables, M. Carter, S. Guntrip, K. Smith, S. McKeown, R. Shaw, P. Topley, L. Thomsen, K. Affleck, A. Jowett, D. Hayes, M. Willson, P. Woollard, D. Spalding, Indazolylamino quinazolines and pyridopyrimidines as inhibitors of the EGFR and C-erbB-2, *Bioorganic & medicinal chemistry letters*, 11 (2001) 1401-1405.

- [38] N. Tebbutt, M.W. Pedersen, T.G. Johns, Targeting the ERBB family in cancer: couples therapy, *Nature reviews. Cancer*, 13 (2013) 663-673.
- [39] G.M. Higa, J. Abraham, Lapatinib in the treatment of breast cancer, *Expert review of anticancer therapy*, 7 (2007) 1183-1192.
- [40] C. Moreira, V. Kaklamani, Lapatinib and breast cancer: current indications and outlook for the future, *Expert review of anticancer therapy*, 10 (2010) 1171-1182.
- [41] E.R. Wood, A.T. Truesdale, O.B. McDonald, D. Yuan, A. Hassell, S.H. Dickerson, B. Ellis, C. Pennisi, E. Horne, K. Lackey, K.J. Alligood, D.W. Rusnak, T.M. Gilmer, L. Shewchuk, A unique structure for epidermal growth factor receptor bound to GW572016 (Lapatinib): relationships among protein conformation, inhibitor off-rate, and receptor activity in tumor cells, *Cancer research*, 64 (2004) 6652-6659.
- [42] S. Bugge, S.J. Kaspersen, S. Larsen, U. Nonstad, G. Bjorkoy, E. Sundby, B.H. Hoff, Structure-activity study leading to identification of a highly active thienopyrimidine based EGFR inhibitor, *European journal of medicinal chemistry*, 75 (2014) 354-374.
- [43] C.N. Cavasotto, M.A. Ortiz, R.A. Abagyan, F.J. Piedrafita, In silico identification of novel EGFR inhibitors with antiproliferative activity against cancer cells, *Bioorganic & medicinal chemistry letters*, 16 (2006) 1969-1974.
- [44] J. Lin, W. Shen, J. Xue, J. Sun, X. Zhang, C. Zhang, Novel oxazolo[4,5-g]quinazolin-2(1H)-ones: dual inhibitors of EGFR and Src protein tyrosine kinases, *European journal of medicinal chemistry*, 55 (2012) 39-48.
- [45] K.G. Petrov, Y.M. Zhang, M. Carter, G.S. Cockerill, S. Dickerson, C.A. Gauthier, Y. Guo, R.A. Mook, Jr., D.W. Rusnak, A.L. Walker, E.R. Wood, K.E. Lackey, Optimization and SAR for dual ErbB-1/ErbB-2 tyrosine kinase inhibition in the 6-furanylquinazoline series, *Bioorganic & medicinal chemistry letters*, 16 (2006) 4686-4691.
- [46] A. Gangjee, W. Li, L. Lin, Y. Zeng, M. Ihnat, L.A. Warnke, D.W. Green, V. Cody, J. Pace, S.F. Queener, Design, synthesis, and X-ray crystal structures of 2,4-diaminofuro[2,3-d]pyrimidines as multireceptor tyrosine kinase and dihydrofolate reductase inhibitors, *Bioorganic & medicinal chemistry*, 17 (2009) 7324-7336.
- [47] R.A. Friesner, R.B. Murphy, M.P. Repasky, L.L. Frye, J.R. Greenwood, T.A. Halgren, P.C. Sanschagrín, D.T. Mainz, Extra precision glide: docking and scoring incorporating a model of hydrophobic enclosure for protein-ligand complexes, *Journal of medicinal chemistry*, 49 (2006) 6177-6196.
- [48] T.A. Halgren, R.B. Murphy, R.A. Friesner, H.S. Beard, L.L. Frye, W.T. Pollard, J.L. Banks, Glide: a new approach for rapid, accurate docking and scoring. 2. Enrichment factors in database screening, *Journal of medicinal chemistry*, 47 (2004) 1750-1759.
- [49] R.A. Friesner, J.L. Banks, R.B. Murphy, T.A. Halgren, J.J. Klicic, D.T. Mainz, M.P. Repasky, E.H. Knoll, M. Shelley, J.K. Perry, D.E. Shaw, P. Francis, P.S. Shenkin, Glide: a new approach for rapid, accurate docking and scoring. 1. Method and assessment of docking accuracy, *Journal of medicinal chemistry*, 47 (2004) 1739-1749.
- [50] E. Yoo, B.M. Crall, R. Balakrishna, S.S. Malladi, L.M. Fox, A.R. Hermanson, S.A. David, Structure-activity relationships in Toll-like receptor 7 agonistic 1H-imidazo[4,5-c]pyridines, *Organic & biomolecular chemistry*, 11 (2013) 6526-6545.
- [51] N. Lougiakis, E.S. Gavriil, M. Kairis, G. Sioupouli, G. Lambrinidis, D. Benaki, E. Kryptou, E. Mikros, P. Marakos, N. Pouli, G. Diallinas, Design and synthesis of purine analogues as highly specific ligands for FcyB, a ubiquitous fungal nucleobase transporter, *Bioorganic & medicinal chemistry*, 24 (2016) 5941-5952.
- [52] T. Georgiou, M. Tofi, T. Montagnon, G. Vassilikogiannakis, A versatile and general one-pot method for synthesizing bis-spiroketal motifs, *Organic letters*, 8 (2006) 1945-1948.
- [53] N.T. Tzvetkov, C.E. Muller, Facile synthesis of 5-amino- and 7-amino-6-azaoxindole derivatives, *Tetrahedron Letters*, 53 (2012) 5597-5601.

- [54] M.C. Liu, M.Z. Luo, D.E. Mozdziesz, T.S. Lin, G.E. Dutschman, E.A. Gullen, Y.C. Cheng, A.C. Sartorelli, Synthesis of halogen-substituted 3-deazaadenosine and 3-deazaguanosine analogues as potential antitumor/antiviral agents, *Nucleosides, nucleotides & nucleic acids*, 20 (2001) 1975-2000.
- [55] Schrödinger, Schrödinger Release 2019-1:MacroModel, in, LLC, New York, NY, 2019.
- [56] S.A. Hitchcock, L.D. Pennington, Structure-brain exposure relationships, *Journal of medicinal chemistry*, 49 (2006) 7559-7583.
- [57] M.N. Martinez, G.L. Amidon, A mechanistic approach to understanding the factors affecting drug absorption: a review of fundamentals, *Journal of clinical pharmacology*, 42 (2002) 620-643.
- [58] O. Argyros, T. Karampelas, X. Asvos, A. Varela, N. Sayyad, A. Papakyriakou, C.H. Davos, A.G. Tzakos, D. Fokas, C. Tamvakopoulos, Peptide-Drug Conjugate GnRH-Sunitinib Targets Angiogenesis Selectively at the Site of Action to Inhibit Tumor Growth, *Cancer research*, 76 (2016) 1181-1192.
- [59] T. Karampelas, O. Argyros, N. Sayyad, K. Spyridaki, C. Pappas, K. Morgan, G. Kolios, R.P. Millar, G. Liapakis, A.G. Tzakos, D. Fokas, C. Tamvakopoulos, GnRH-Gemcitabine conjugates for the treatment of androgen-independent prostate cancer: pharmacokinetic enhancements combined with targeted drug delivery, *Bioconjugate chemistry*, 25 (2014) 813-823.
- [60] T. Karampelas, E. Skavatsou, O. Argyros, D. Fokas, C. Tamvakopoulos, Gemcitabine Based Peptide Conjugate with Improved Metabolic Properties and Dual Mode of Efficacy, *Molecular pharmaceutics*, 14 (2017) 674-685.
- [61] O. Argyros, T. Karampelas, A. Varela, X. Asvos, A. Papakyriakou, A. Agalou, D. Beis, C.H. Davos, D. Fokas, C. Tamvakopoulos, Targeting of the breast cancer microenvironment with a potent and linkable oxindole based antiangiogenic small molecule, *Oncotarget*, 8 (2017) 37250-37262.